Ph.D. Dissertation of Medical Science

# Pleiotropic Effects of Angiotensin II Type 1 Receptor Blocker and Sodium-Glucose Cotransporter Inhibitor on Cardiovascular Diseases

## 심혈관 질환에 대한 Angiotensin II type 1 receptor blocker와 Sodium-glucose cotransporter inhibitor의 다면 발현 효과

February 2023

College of Medicine
Seoul National University
Microbiology and Immunology

Inho Kim

# Pleiotropic Effects of Angiotensin II Type 1 Receptor Blocker and Sodium-Glucose Cotransporter Inhibitor on Cardiovascular Diseases

Advisor: Prof. Seung-Hyeok Seok

Submitting a Ph.D. Dissertation of
Medical Science

October 2022

College of Medicine
Seoul National University
Microbiology and Immunology

Inho Kim

Confirming the Ph.D. Dissertation written by
Inho Kim

January 2023

| | | |
|---|---|---|
| Chair | Hae-Young Lee | (Seal) |
| Vice Chair | Seung-Hyeok Seok | (Seal) |
| Examiner | Hyun-Jai Cho | (Seal) |
| Examiner | Jinki Yeom | (Seal) |
| Examiner | Seong-Mi Park | (Seal) |

# Pleiotropic Effects of Angiotensin II Type 1 Receptor Blocker and Sodium–Glucose Cotransporter Inhibitor on Cardiovascular Diseases

지도교수 석 승 혁

이 논문을 의학박사 학위논문으로 제출함

2022년 10월

서울대학교 대학원

의학과 미생물학 전공

김 인 호

김인호의 의학박사 학위논문을 인준함

2023년 1월

위 원 장 이 해 영 (인)

부위원장 석 승 혁 (인)

위 원 조 현 재 (인)

위 원 염 진 기 (인)

위 원 박 성 미 (인)

# Abstract

Understanding the molecular mechanisms underlying the pleiotropic effects of drugs is important for optimizing drug use and may further contribute to the understanding of disease pathogenesis as well as the development of novel therapies. Here I studied the pleiotropic effects of Angiotensin II (Ang II) type 1 receptor blocker (ARB) and sodium-glucose cotransporter (SGLT) inhibitors on cardiovascular events in vascular aging and diabetes.

In Chapter 1, the anti-senescence effect of Fimasartan (FIMA), a novel ARB, on the mechanism of Ang II induced-cellular senescence was investigated. Angiotensin II (Ang II) has been suggested to accelerate vascular senescence; however, the molecular mechanisms remain unknown. Ang II-treated human coronary artery smooth muscle cells (hCASMCs) were significantly increased senescence-associated $\beta$-galactosidase (SA-$\beta$-gal) positive cells. However, cellular senescence induced by Ang II was significantly attenuated by pretreatment with the FIMA. The expressions of p53 and p16, senescence regulator, were significantly increased by Ang II and suppressed by FIMA. Cellular communication factor 1 (CCN1) was rapidly induced by Ang II. Compared with the control, CCN1 overexpressed hCASMCs by Ad-

CCN1 viral vector transfection showed significantly increased SA-β-gal-positive cells. Upon CCN1 suppression by Ad-AS-CCN1 transfection, Ang II-induced senescence was significantly decreased. The p53 expression by Ang II was significantly attenuated by Ad-AS-CCN1, whereas p16 expression was not regulated. Ang II activated ERK1/2 and p38 MAPK, which was significantly blocked by FIMA. ERK and p38 inhibition both regulated Ang II-induced CCN1 expression. However, p53 expression was only regulated by ERK1/2, whereas p16 expression was only attenuated by p38 MAPK. In conclusion, Ang II induced hCASMCs senescence by the ERK/p38 MAPK-CCN1-p53 pathway, and FIMA protected against Ang II-induced cellular senescence.

In Chapter 2, cardioprotective effects and molecular mechanism of SGLT2 inhibitor, Empagliflozin (EMPA), and dual SGLT1/2 inhibitor, Sotagliflozin (SOTA), in diabetes mellitus (DM)-associated heart failure (HF) were studied. DM-HF causes high morbidity and mortality. SGLT inhibitors are emerging as HF medication beyond their glucose lowering efficacy. However, the precise mechanism underlying this cardioprotective effect has not yet been elucidated. Here, I evaluated the effects of EMPA and SOTA in a novel zebrafish larvae model for DM combined with HF with reduced ejection fraction (DM-HFrEF). The myocardial

contractile functions, motility and survival were evaluated. DM-HFrEF zebrafish larvae showed impaired cardiac contractility and decreased motility and survival, all of which were improved by EMPA or SOTA treatment. However, the high molarity of SOTA treatment group had worse survival rates and less motility preservation than the EMPA treatment group with the same concentration, and an epicardial edema and uninflated swim bladder were observed. The structural binding and modulating effect of the two medications on sodium-hydrogen exchanger 1 (NHE1) was evaluated *in silico* and *in vitro*. The SOTA, EMPA and Cariporide (CARI) showed a similar structural binding affinity to NHE1 *in silico* and *in vitro*. In addition, EMPA, SOTA, and CARI effectively reduced intracellular $H^+$, $Na^+$ and $Ca^{2+}$ changes through the inhibition of NHE1 activity, and no NHE1 inhibitory effect of EMPA or SOTA was observed in cells pretreated with CARI. These findings suggest that both EMPA and SOTA exert cardioprotective effect in DM-HFrEF zebrafish model through the inhibition of NHE1 activity. In addition, despite the similar cardioprotective effects of both drugs, SOTA may be less effective than EMPA at high concentrations.

Keyword: Pleiotropic effect, Senescence, Diabetes mellitus, Heart failure

Student Number: 2017−24875

# General introduction

Cardiovascular diseases (CVDs) are a group of cardiac and vascular disorders and are the leading cause of death worldwide. According to the World Health Organization (WHO), approximately 17.9 million people died from CVDs in 2019, accounting for 32% of global deaths. Of these, 85% died from heart attacks and strokes. In addition, CVDs accounted for 38% of the 17 million deaths under the age of 70 from noncommunicable diseases in 2019. CVDs therefore account for a significant amount of suffering and health care expenditure[1-4]. Although the quality of treatment for CVDs has improved significantly over the past decade, the prognosis is still poor. Therefore, many studies are needed to improve long-term outcomes and implement effective treatments.

The term pleiotropy comes from the Greek *pleion* meaning "more" and *tropos* meaning "turn"[5]. In the past 20 years, the pleiotropic effects of drugs have aroused great interest among experimental and clinical researchers. The pleiotropic action is defined as multiple effects derived from a single gene, and in pharmacological terms, it exhibits additional effects observed, ie, additional effects other than the purpose for which the agent was specifically developed[6]. Because pleiotropic effects may not be related to the

main mechanism of action of drugs and are generally not easy to predict, they may not be accurately detected in preclinical studies. Therefore, understanding the mechanisms underlying the pleiotropic effects of drugs is important for optimizing drug use and may further contribute to the understanding of disease pathogenesis as well as the development of novel therapies. Recently, the pleiotropic activity associated with cardiovascular risk reduction of various drugs, such as Angiotensin II type 1 receptor blocker (ARB)[7], Beta-blocker[8], Angiotensin-converting enzyme (ACE) inhibitor[9], Statin[10], DPP-4 inhibitor[11], Metformin[12] and SGLT2 inhibitor[13] has been intensively studied. Considering the importance of the pleiotropic properties of drugs, it can be expected that in the future, they will be characterized by intensive studies on the pleiotropic effects of several drug classes used for the treatment of CVDs.

Here, I discuss the anti-senescence effect of ARB on Angiotensin II-induced coronary artery aging[14], and the cardioprotective effect of SGLT inhibitors on diabetic heart failure. I strongly believe that a comprehensive understanding of the pleiotropic effects of both drugs, based on these studies, can provide insight into cardiovascular disease and the basis for novel treatment strategies in the future.

# Table of contents

# List of figures

## Chapter 1

## Chapter 2

# List of abbreviations

## Chapter 1

**Ang II:** Angiotensin II

**Ad-AS-CCN1:** Adenoviral vectors expressing antisense CCN1

**Ad-CCN1:** Adenoviral vectors expressing CCN1

**Ad-GFP:** Adenoviral vector expressing green fluorescence proteins

**ARB:** Ang II type 1 receptor blocker

**AT1R:** Ang II type 1 receptor

**CVD:** Cardiovascular disease

**CCN1:** Cellular communication network factor 1

**FIMA:** Fimasartan

**GAPDH:** Glyceraldehyde 3-phosphate dehydrogenase

**hCASMC:** Human coronary artery smooth muscle cell

**NADPH:** Nicotinamide adenine dinucleotide phosphate

**ns:** Not significant

**PCR:** Polymerase chain reaction

**RAS:** Renin-angiotensin system

**SA-β-gal:** Senescence-associated β-galactosidase

**SDS:** Sodium dodecyl sulfate

**VSMC:** Vascular smooth muscle cell

## Chapter 2

CARI: Cariporide

DARTS: Drug affinity responsive target stability

DM: Diabetes mellitus

EMPA: Empagliflozin

GLU: D-glucose

HF: Heart failure

NHE: Sodium-hydrogen exchanger

SD: Standard deviation

SGLT: Sodium-glucose cotransporter

SOTA: Sotagliflozin

STZ: Streptozotocin

TER: Terfenadine

VEH: Vehicle

vFS: Ventricular fractional shortening

# Chapter 1

# Angiotensin II type 1 receptor blocker, Fimasartan, Reduces Cellular Senescence of Coronary Artery Smooth Muscle Cells by inhibiting the CCN1 Signaling Pathway

# Introduction

Aging is one of the major risk factors for cardiovascular diseases (CVDs)[15]. The incidence of CVDs, the leading cause of death globally, continues to rise as life expectancy increases[1-4]. Cellular senescence due to aging is strongly associated with the onset and progression of CVDs. In particular, cellular senescence in coronary arteries is a very dangerous factor for ischemic heart failure[16]. Various stimuli including DNA damage, telomere dysfunction and oxidative stress have been reported to rapidly induce cellular senescence[17]. Moreover, clinical risk factors such as inflammation, hypertension, obesity and diabetes were reported to accelerate vascular senescence, so-called early vascular aging[18]. Senescent cells maintain cell viability but shorten telomere length and decrease proliferation[19]. They also feature a phenotypically enlarged, flattened morphology and accumulated senescence-associated $\beta$-galactosidase (SA-$\beta$-gal)[20]. In addition, senescent cells express a diverse set of genes, such as p53 and p16, which serve as negative regulators of the cell cycle and markers of cellular senescence[21].

The renin-angiotensin system (RAS) plays an important role in the regulation of renal, cardiac, and vascular physiology.

Maladaptive activation of RAS has been shown to play a central role in the pathogenesis of CVDs of various etiologies, including hypertension, heart failure, and diabetes[22, 23]. Angiotensin II (Ang II) is a potent systemic vasoconstrictor and is involved in several vascular pathologies by promoting pathologic hypertrophy, fibrosis, extracellular matrix deposition and inflammation via Ang II type 1 receptor (AT1R)[24-26]. There is some evidence suggesting the role of Ang II in vascular senescence and the protective effect of RAS inhibition against it[27-30]. AT1R blockers (ARBs) are mainly used for the treatment of hypertension and have been reported to exert pleiotropic effects to protect against oxidative and inflammatory actions[31-33]. Fimasartan (FIMA) is a new ARB with a selective AT1R blocking effect[34]. Recent studies have reported the pleiotropic effect of FIMA beyond blood pressure lowering in myocardial infarction, heart failure and inflammatory response[35-37].

Cellular communication network factor 1 (CCN1) is a one of downstream molecule of AT1R[38]. CCN1 is the first member of the CCN family of secreted extracellular matrix proteins in mammals[39]. CCN1 was originally cloned as an immediate early gene expressed in fibroblasts after growth factor stimulation[40]. CCN1 expression has been reported to be associated with vascular

restenosis, angiogenesis, and tumor growth[41]. Also, CCN1 blockade inhibits vascular smooth muscle cell (VSMC) proliferation and neointimal hyperplasia[42]. Several recent studies have confirmed a high correlation between CCN1 expression and cellular senescence[43-45].

Therefore, in this study, I evaluated anti-senescent effect of FIMA in Ang II-induced coronary artery smooth muscle cell senescence, and hypothesized that FIMA suppresses cellular senescence by regulating the expression of CCN1. In addition, I analyzed the protective mechanisms of FIMA related to CCN1 expression in Ang II-induced vascular senescence.

# Materials and methods

## Reagents and antibodies

Ang II was purchased from Sigma-Aldrich (Louis, MO, USA). PD98059, ERK1/2 inhibitor, and SB203580, p38 MAP kinase inhibitor, were purchased from Invitrogen (Carlsbad, CA, USA). Fimasartan was provided by Boryung Pharmaceutical Co., Ltd (Seoul, Korea). Primary antibodies against p53, p16 and $\beta$-actin antibodies were purchased from Santa Cruz Biotechnology (Dallas, TX, USA), and Phospho-ERK1/2, ERK1/2, Phospho-p38 MAPK and p38 MAPK antibodies were purchased from Cell Signaling Technology (Danvers, MA, USA). CCN1 antibody was purchased from Abcam (Cambridge, UK). Secondary antibodies were purchased from Santa Cruz Biotechnology (Dallas, TX, USA).

## Cell culture and adenoviral vectors

Human coronary artery smooth muscle cells (hCASMCs) were purchased from Lonza (Basel, Switzerland). Six- to eight-passage hCASMCs were cultured in SMC growth medium consisting of basal media, insulin, human recombinant epidermal growth factor, human recombinant fibroblast growth factor, gentamicin, amphotericin, and 5% fetal bovine serum at 37° C in an atmosphere of 95% air and

5% $CO_2$ based on manufacturer's recommendations. Recombinant adenoviral vectors, expressing *CCN1* cDNA (Ad-CCN1) or antisense *CCN1* cDNA (Ad-AS-CCN1) fragments, were used for the overexpression or suppression of *CCN1* gene in cultured hCASMCs. As a control, an adenoviral vector expressing green fluorescence proteins only (Ad-GFP) was used.

### SA-β-gal staining assay

Cellular senescence was examined by SA-β-gal activity using Senescence Detection Kit (Calbiochem, Merck Millipore, Darmstadt, Germany). Briefly, cultured hCASMCs were wash with PBS and fixed with Fixative Solution at room temperature for 15 minutes and washed with PBS again. Then fixed cells were incubated with Staining Solution Mix at 37° C overnight. Cellular images were acquired with a fluorescence microscope (DM 5500B, Leica Microsystems, Wetzlar, Germany) using a digital imaging system (DFC360FX, LEICA). SA-β-gal positive cells were counted per 50 cells and normalized to vehicle treated cells.

### Total RNA isolation and quantitative real-time polymerase chain reaction (qRT-PCR)

Cultured hCASMCs were washed twice with PBS and cell pellets

were collected for RNA isolation. And total RNA was isolated from the cell pellets by the RNeasy mini-Kit (Qiagen, Hilden, Germany) and reverse transcribed using the amfiRivert cDNA Synthesis Premix (GenDEPOT, Katy, TX, USA) based on manufacturer's instructions. Quantitative PCR performed using SYBR Green PCR kit (Applied Biosystems, Waltham, MA, USA) and StepOnePlus Real-Time PCR System (Applied Biosystems, Waltham, MA, USA). Real-time PCR was performed with *glyceraldehyde 3-phosphate dehydrogenase* (*GAPDH*) primers (forward: 5′ -GGA AGG TGA AGG TCG GAG TC-3′ , reverse: 5′ -GAA GGG GTC ATT GAT GGC AAC-3′ ), *CCN1* primers (forward: 5′ -TCT CGT TGC TGC TCA TGA AAT T-3′ , reverse: 5′ -TAG AGT GGG TAC ATC AAA GCT TCA G-3′ ), *p53* primers (forward: 5′ -GCC CAA CAA CAC CAG CTC CT-3′ , reverse: 5′ -CCT GGG CAT CCT TGA GTT CC-3′ ) and *p16* primers (forward: 5′ -CCC AAC GCA CCG AAT AGT TA-3′ , reverse: 5′ -ACC AGC GTG TCC AGG AAG -3′ ). All genes were normalized to the *GAPDH* mRNA level.

## Immunoblotting

Cultured hCASMCs with the indicated reagents were washed twice with PBS and collected. Cell pellets were lysed in RIPA cell lysis buffer (Santa Cruz Biotechnology, Dallas, TX, USA), and protein

concentration was determined by BCA protein assay (Thermo Fisher Scientific, Waltham, MA, USA). The 30 μg of proteins were loaded and separated on 8% or 10% sodium dodecyl sulfate-polyacrylamide gels and transferred to activated polyvinylidene fluoride membranes (Immobilon-P; Merck Millipore, Darmstadt, Germany) by methanol. The transferred membranes were blocked with blocking buffer (5% skim milk in TBST) at room temperature for 60 minutes and incubated with the indicated primary antibodies in blocking buffer overnight at 4° C. The membranes were washed three times with TBST and incubated at room temperature with secondary antibodies conjugated to horseradish peroxidase at 1:2,500 for 60 minutes in TBST with 2% skim milk and washed three times again. Proteins were detected using enhanced chemiluminescence detection reagents (Promega, Madison, WI, USA) and the protein levels were acquired through densitometric scanning. Obtained values were expressed in arbitrary densitometric units and normalized to those of β-actin to correct for total protein loading.

### Statistical analysis

All data were presented as mean ± standard deviation. Statistical analyses were performed with GraphPad Prism (GraphPad Software,

San Diego, CA, USA) using the student's t-test for comparing 2 groups or one-way analysis of variance followed by the Turkey post hoc test for comparing >2 groups. A probability value of less than 0.05 was considered statistically significant.

# Results

## Angiotensin II induces cellular senescence in hCASMCs, whereas Fimasartan inhibits it.

I treated hCASMCs with 1 to 100 nM of Ang II and evaluated cellular senescence by counting SA-β-gal-positive cells. Ang II treatment for 7 days significantly increased SA-β-gal-positive cells at 10 nM (2.63±0.75-fold) and at 100 nM (3.31±0.26-fold) compared with the control (Figure 1A and B). In contrast, Ang II-induced SA-β-gal activity (5.77±1.05-fold vs. the control) was significantly inhibited by pretreatment with 1 μM of FIMA (2.0±0.53-fold vs. the control with Ang II, Figure 1C and D).

Next, I evaluated the expression levels of p53 and p16, cellular senescence regulators, following Ang II treatment by immunoblot analysis and qRT-time PCR[27]. Both p53 and p16 protein expressions were significantly increased (p53: 1.39±0.17, p16: 1.19±0.10-fold vs. the control, Figure 2A-C) and their mRNA levels were similarly increased (*p53*: 3.20±0.78, *p16*: 7.79±1.01-fold vs. the control, Figure 2D and E), while these Ang II-induced increases were completely inhibited in both protein (p53: 1.02±0.12, p16: 0.96±0.07-fold vs. the control, Figure 2A-C) and mRNA by treatment with FIMA (*p53*: 0.15±0.13, *p16*: 0.27±0.22-

fold vs. the control, Figure 2D and E).

These observations suggest that Ang II promotes the hCASMCs senescence via accumulated stress through the AT1R-p53/p16 dependent pathway, and FIMA blocks the AT1R to regulate hCASMCs senescence.

## Angiotensin II-induced CCN1 promotes cellular senescence via AT1R-p53-dependent pathway

It was previously reported that the expression of CCN1 is induced by Ang II, and CCN1 was reported to induce cellular senescence[43]. Therefore, I investigated whether CCN1 mediates Ang II-induced cellular senescence in hCASMCs. First, I performed qRT-PCR to assess the *CCN1* gene transcription on Ang II-treated hCASMCs. The *CCN1* mRNA expression levels were increased in Ang II-treated hCASMCs over 10 nM (10 nM: 1.52±0.27, 100 nM: 1.54±0.28-fold vs. the control, Figure 3A). Ang II rapidly induced *CCN1* mRNA expression within 30 minutes (1.5±0.34-fold vs. the control) and peaked at 120 minutes (3.1±0.80-fold vs. the control, Figure 3B). Conversely, Ang II-induced *CCN1* mRNA expression (1.55±0.36-fold. vs. the control) was completely inhibited by FIMA (0.95±0.23-fold vs. the control, Figure 3C).

I investigated whether CCN1 directly induces hCASMCs

senescence. For the overexpression or the suppression of CCN1, I used a replication adenovirus encoding CCN1-specific cDNA (Ad-CCN1) or CCN1-specific antisense cDNA (Ad-As-CCN1) fragments. In CCN1-overexpressed hCASMCs, SA-$\beta$-gal positive(+) cells were significantly increased (3.47±0.65-fold vs. the control transfected with Ad-GFP, Figure 4A and B). Conversely, when CCN1 expression was blocked with Ad-AS-CCN1, Ang II-induced SA-$\beta$-gal positive(+) cell numbers were significantly decreased (Ang II-treated hCASMC with Ad-GFP: 3.73±0.23 and Ang II-treated hCASMC with Ad-As-CCN1: 1.77±0.60-fold vs. the vehicle-treated hCASMC with Ad-GFP, Figure 4C and D).

The p16 and p53 were reported to be involved in different pathways of cellular senescence[21]. Therefore, I examined whether CCN1-induced hCASMC senescence was related to the p16- or p53-dependent pathway. In Ad-CCN1 transfected hCASMCs, expression of CCN1 and p53 were significantly increased (CCN1: 37.94±3.26-fold, p53: 1.57±0.16-fold vs. the control transfected with Ad-GFP, Figure 5A-C), whereas p16 expression was not changed in protein (p16: 0.95±0.10-fold vs. the control transfected with Ad-GFP, Figure 5A and D) and mRNA (*CCN1*: 3.23±0.60-fold, *p53*: 11.90±1.18-fold, *p16*: 1.03±0.40-fold vs. the control transfected with Ad-GFP, Figure 5E-G). In

addition, the p53 expression was increased by CCN1 in a dose-dependent manner (25 MOI: 1.36-fold, 125 MOI: 1.42-fold, 250 MOI: 1.71-fold vs. the control transfected with Ad-GFP, Figure 6A-C). However, in CCN1-suppressed hCASMCs by Ad-As-CCN1 transfection (Figure 7A and B), p53 expression was significantly suppressed (Figure 7A and C), whereas p16 expression was not changed (Figure 7A and D). This tendency was also observed in the hCASMCs treated with Ang II, and suppression of CCN1 expression in hCASMC by Ad-As-CCN1 (Figure 8A and B) significantly reduced p53 (Figure 8A and C) but had no effect on p16 (Figure 8A and D).

These results showed that Ang II induced CCN1 via AT1R and CCN1 mediated Ang II-induced hCASMCs senescence. Also, CCN1-induced cellular senescence was mediated by the p53-dependent pathway, not by the p16-dependent pathway.

## Ang II induces CCN1 expression through the ERK/p38 MAPK signaling pathway

Lastly, I investigated the mechanisms of CCN1-associated Ang II dependent hCASMCs senescence in more detail. It was previously reported that Ang II-related cellular senescence was contributed to by MAPK, such as ERK1/2 and p38 MAPK[39]. Based on these

reports, I investigated the role of ERK/p38 MAPK pathways in CCN1-mediated hCASMCs senescence. First, I evaluated ERK1/2 and p38 MAPK activation by measuring phosphorylation in Ang II-treated hCASMCs. As expected, phosphorylation levels of ERK1/2 (Figure 9A and B) and p38 (Figure 9A and C) were increased by Ang II and blocked by FIMA pretreatment (Figure 9A–C). Next, I evaluated cellular senescence pathway in the presence of either PD98059, an ERK1/2 inhibitor, or SB203580, a p38 MAPK inhibitor, in Ang II-stimulated hCASMCs (Figure 10A-F). Immunoblot analysis showed that the inhibition of ERK1/2 by PD98059 attenuated the expression of both CCN1 and p53 but not p16, whereas p38 MAPK inhibition by SB203580 attenuated CCN1, p16 and p53 (Figure 10A-F). These data showed that CCN1 was downstream of ERK1/2 and p38 MAPK, and directly controlled p53 expression, but not p16 in Ang II-induced hCASMCs senescence. The proposed signaling pathways of Ang II-induced hCASMCs senescence were summarized in Figure 11.

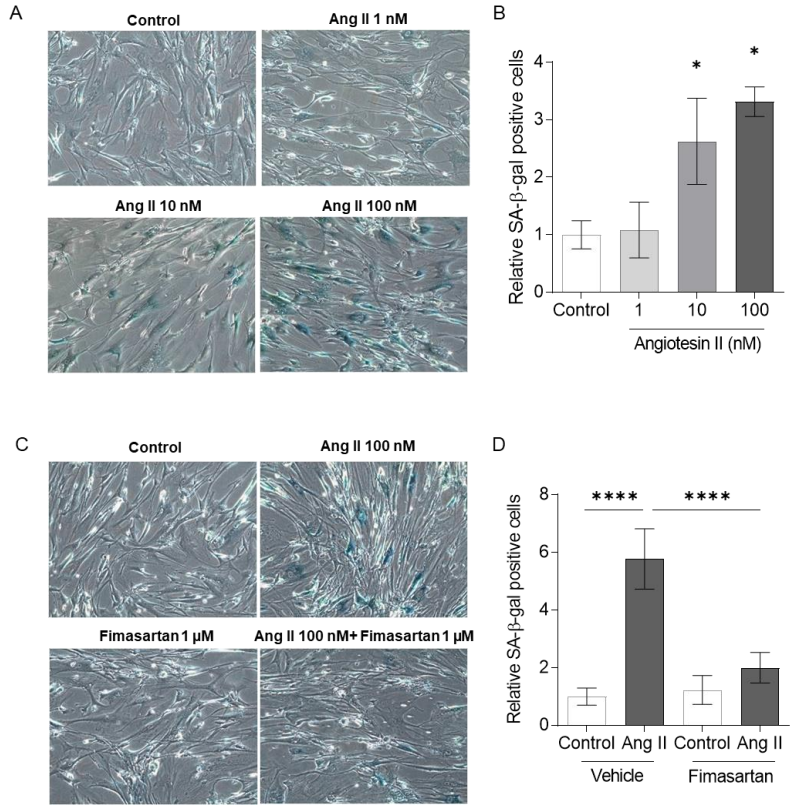


**Figure 1.** Angiotensin II-induced cellular senescence in hCASMC and the anti-senescence effect of Fimasartan. (A and B) Counting SA-$\beta$-gal positive cells following treatment with Ang II (1-100 nM) for 7 days. (C and D) Counting SA-β-gal positive cells after fimasartan treatment (1 μM). Values are given as mean±standard deviation. $^{**}p < 0.01$, $^{****}p < 0.0001$.

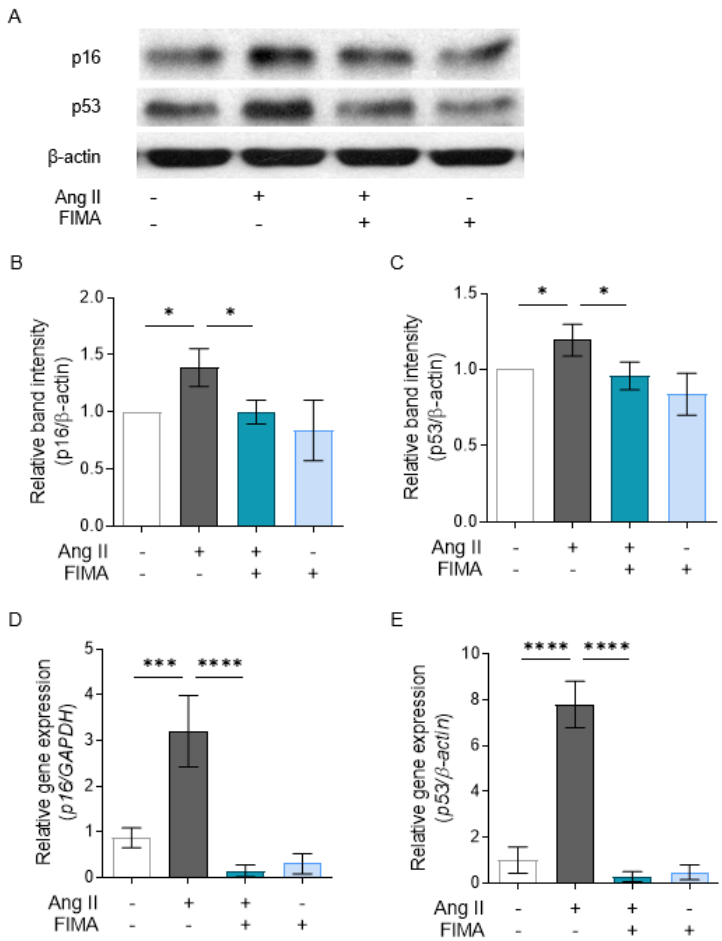


**Figure 2.** Induction of p53 and p16 expression by Angiotensin II and inhibitory effect of Fimasartan. (A–C) Protein and (D and E) mRNA expression of (A, B and D) p16 and (A, C and E) p53 after Ang II and/or Fimasartan treatment. Values are given as mean±standard deviation. $*p < 0.05$, $***p < 0.001$, $****p < 0.0001$.

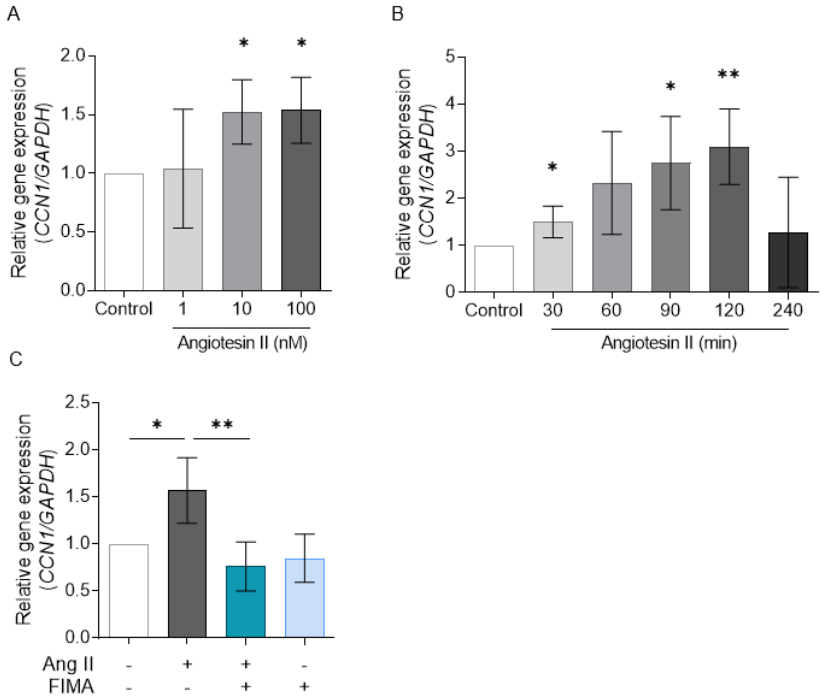


**Figure 3.** Induction of gene expression of CCN1 by Angiotensin II and inhibition by Fimasartan. (A) CCN1 mRNA expression following Ang II treatment in a concentration-dependent manner (1-100 nM, 120 minutes). (B) Induced CCN1 mRNA expression by 100 nM Ang II in a time-dependent manner (30-120 min). (C) Inhibition of CCN1 mRNA by pretreatment with Fimasartan (1 μM). Values are given as mean±standard deviation. $*p < 0.05$, $**p < 0.01$.

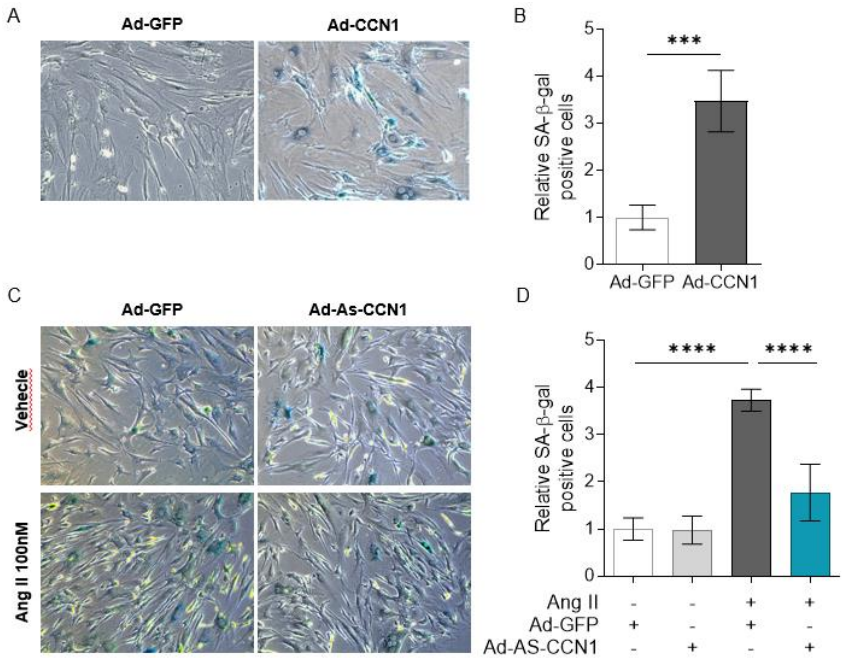


**Figure 4.** CCN1 regulates cellular senescence in hCASMCs. (A and B) Counting SA-$\beta$-Gal positive cells in hCSMS after Ad-CCN1 transfection. (C and D) Counting SA-β-Gal positive cells in hCSMS after Ang II treatment and/or Ad-AS-CCN1 transfection. Values are given as mean±standard deviation. ***$p < 0.001$, ****$p < 0.0001$.

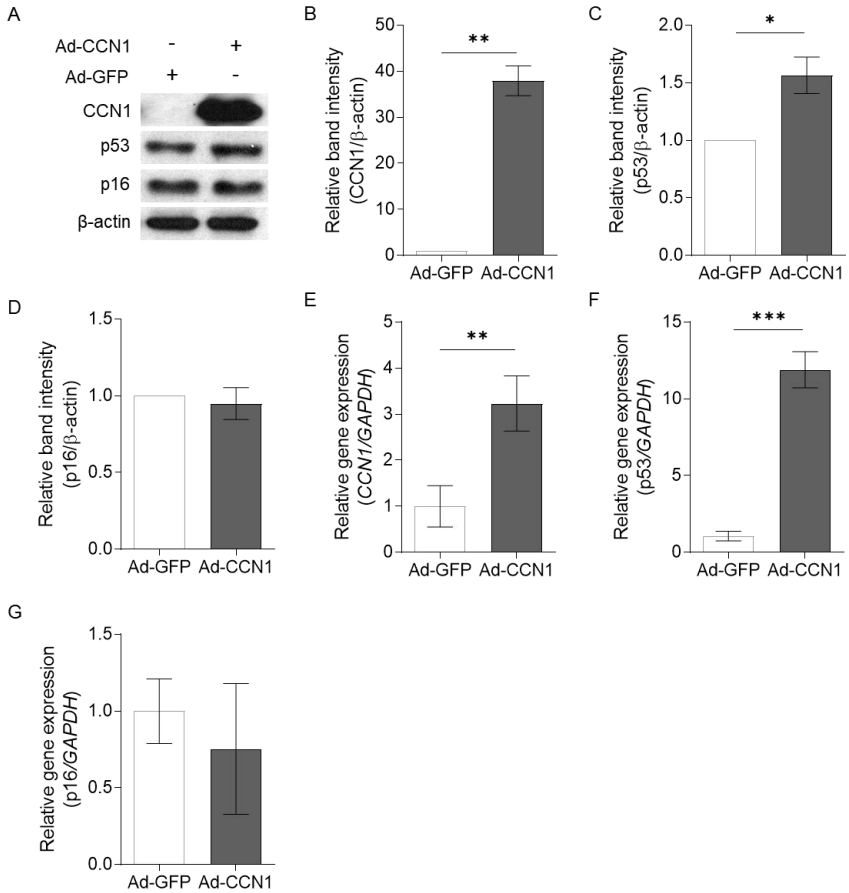


**Figure 5.** Changes in expression of senescence-associated markers p53 and p16 according to CCN1 expression induction. (A, B) Protein and (E) gene expression levels of CCN1 after Ad-CCN1 transfection (50 MOI). Changes in expression of (A, C and F) p53 and (A, D and G) p16 after induction of CCN1 expression with Ad-CCN1. Values are given as mean±standard deviation. $*p < 0.05$, $**p < 0.01$, $***p < 0.001$.

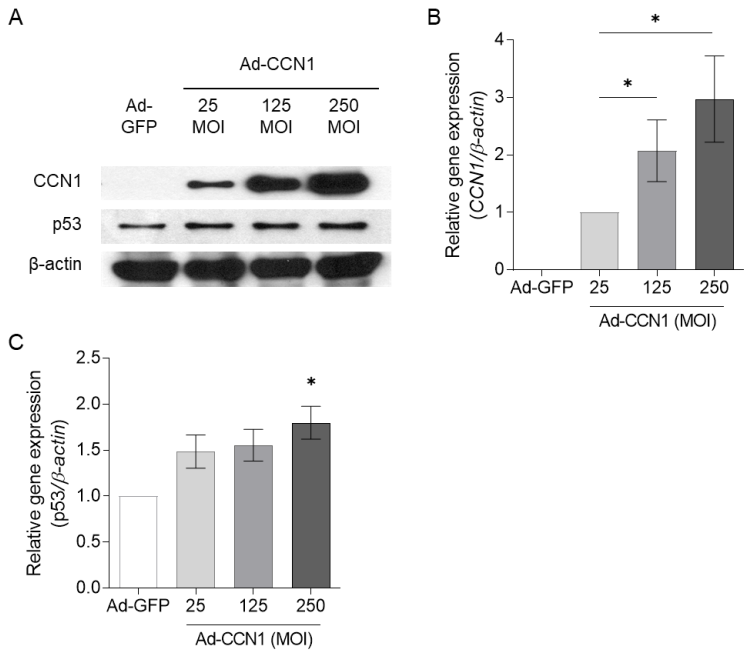


**Figure 6.** Changes in p53 expression according to CCN1 expression level. (A and B) CCN1 and (C) p53 protein expression level following Ad-CCN1 transfection in a MOI-dependent manner. Values are given as mean±standard deviation. $*p < 0.05$.

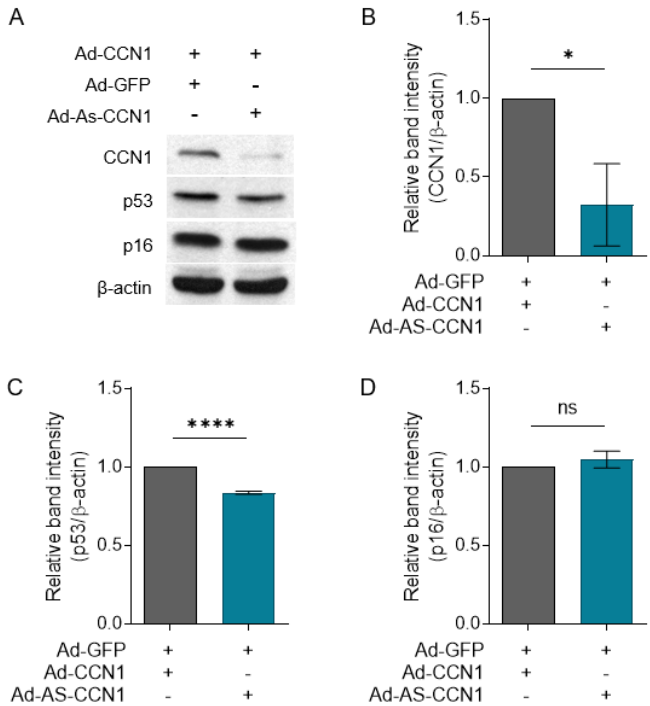


Figure 7. Changes in expression of senescence-associated markers p53 and p16 according to CCN1 suppression. (A, B) expression levels of CCN1, (A and C) p53 and (A and D) p16 after Ad-CCN1 or Ad-AS-CCN1 transfection (50 MOI). Values are given as mean ±standard deviation. *$p < 0.05$, ****$p < 0.0001$.

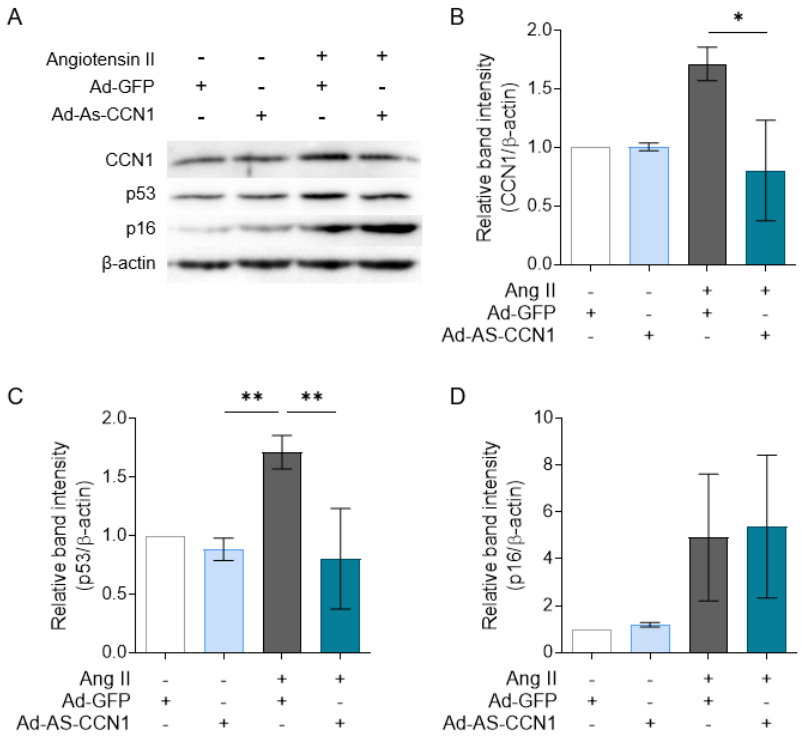


**Figure 8.** Changes in the expression of senescence-associated markers p53 and p16 following CCN1 inhibition in angiotensin II-induced senescence. (A, B) expression levels of CCN1, (A and C) p53 and (A and D) p16 after Ang II and/or Ad-AS-CCN1 transfection (50 MOI). Values are given as mean±standard deviation. $*p < 0.05$, $**p < 0.01$.

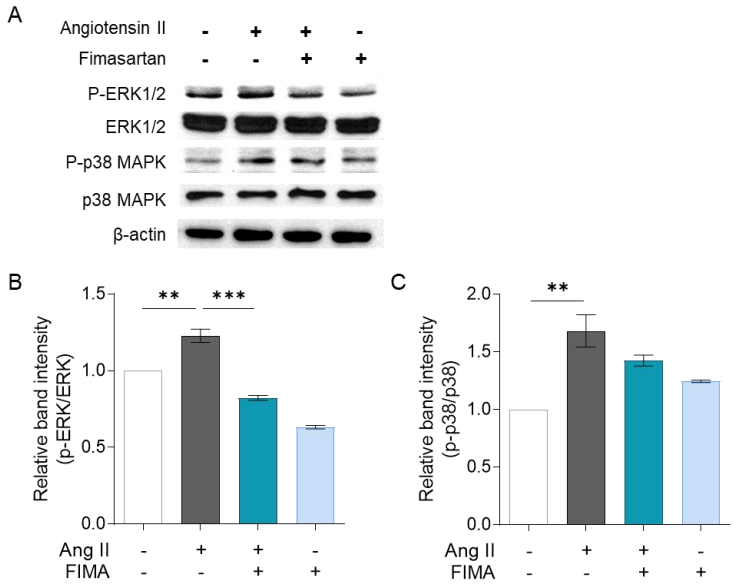


**Figure 9.** Angiotensin II–induced cellular senescence inhibition by fimasartan via ERK/p38 MAPK/CCN1 signaling pathway. (A and B) Changes in phosphorylation of ERK and (C) p38 by Ang II and/or fimasartan treatment. Values are given as mean±standard deviation. $^{**}p < 0.01$, $^{***}p < 0.001$.

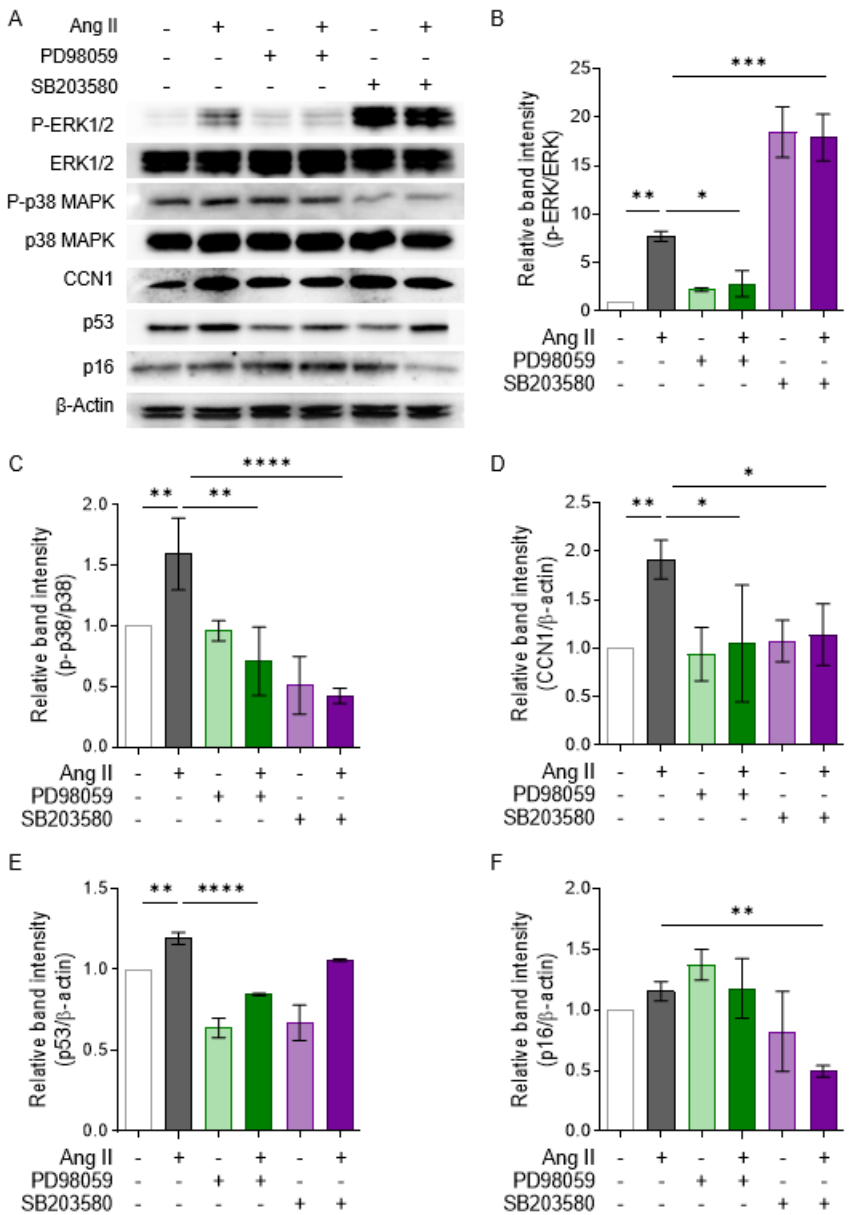


**Figure 10.** Angiotensin II–induced cellular senescence via ERK/p38 MAPK/CCN1 signaling pathway. (A and B) Changes in phosphorylation of ERK and (C) p38 after ERK inhibitor, PD98059, or p38 inhibitor, SB203580, treatment in Ang II–treated hCASMCs. (D) Expression of CCN1, (E) p53 and (F) p16 after treatment with

ERK inhibitor, PD98059, and p38 inhibitor, SB203580, in Ang II-induced cellular senescence. Values are given as mean±standard deviation. *$p < 0.05$, **$p < 0.01$, ***$p < 0.001$, ****$p < 0.0001$,

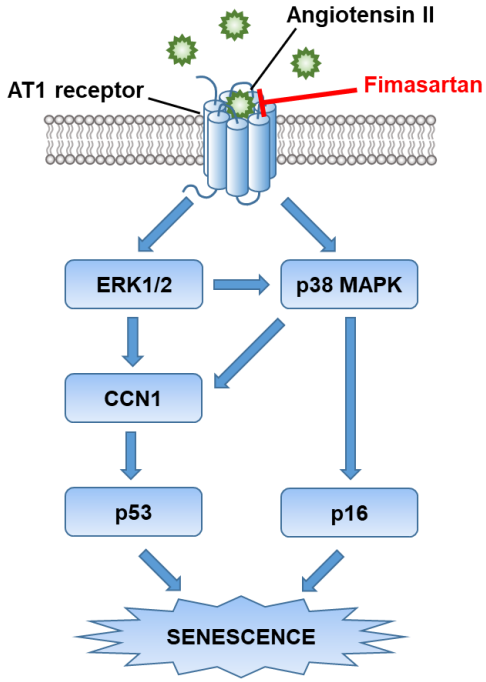


**Figure 11.** The proposed signaling pathways of Angiotensin II-induced hCASMCs senescence. CCN1 is a molecule that regulates p53 in AngII-induced cellular senescence, and Fimasartan may contribute to anti-senescence effects by inhibiting AT1R/ERK/p38 MAPK/CCN1/p53 signaling pathway.

# Discussion

In this study, I demonstrated that FIMA inhibits Ang II-induced hCASMC senescence through the CCN1-mediated signaling pathway. Ang II, through activating ERK1/2, p38 MAPK, p16 and p53, induces vascular senescence, and CCN1 is mediates between ERK1/2 and p53. Therefore, ERK1/2-CCN1-p53 signaling axis may be a crucial pathway regulating Ang II-induced hCASMC senescence (Figure 11).

Vascular aging is characterized by changes in vascular structure and functions including intimal thickening and medial stiffness[46]. VSMCs are the primary cell type in the tunica media, and the status of VSMCs can influence the structure and the function of blood vessels. Previous reports suggested several mechanisms for the promotion of stress-induced vascular cell senescence by Ang II. For example, Ang II activating intracellular reactive oxygen species generation-mediated nicotinamide adenine dinucleotide phosphate (NADPH) oxidase which in turn activates several MAPKs such as ERK1/2 and p38 MAPK, thus leading to the promotion of vascular senescence[47], and oxidative stress induced by Nox1-based NADPH oxidase and mitochondria playing important roles in Ang II-induced cellular senescence[48].

Here, I showed that Ang II significantly induced hCASMC senescence via CCN1 expression and ARB, Fimasartan (FIMA), near completely inhibited CCN1-mediated cellular senescence. Given these findings, I proposed that Ang II induces hCASMC senescence via accumulated stress through CCN1 and ERK/p38 MAPK/p53 signaling pathway, and AT1R blocking effectively regulates VSMC senescence.

The main purpose of this study was to investigate molecular mechanism of Ang II-dependent coronary artery cell senescence, and anti-senescent effect of FIMA. I clearly showed FIMA completely blocks Ang II-induced senescence in hCASMCs. Moreover, I showed that CCN1 has important role in previously known Ang II-induced cellular senescence mechanisms. However, in order to clinically apply these results, I need to confirm the role of CCN1 and effect of FIMA in animal experiments. Therefore, in future studies, it is necessary to confirm the role of CCN1 and the effect of FIMA using the Ang II-induced animal aging model.

In conclusion, I showed that Ang II induced hCASMC senescence via CCN1 and ERK/p38 MAPK/p53 signaling pathway, and FIMA suppressed Ang II-induced hCASMC senescence. These results provide the evidence that blockade of CCN1 may contributes to suppression of vascular aging and CVDs.

Chapter 2

# Comparison of the Effects of Empagliflozin and Sotagliflozin on a Zebrafish Diabetic Heart Failure with Reduced Ejection Fraction Model

# Introduction

The prevalence of diabetes mellitus (DM) is rapidly increasing worldwide. The number of people with DM worldwide is over 425 million and is expected to reach 700 million by 2045[49]. DM is strongly associated with cardiovascular disease (CVD). Among CV complications, heart failure (HF) increases significantly in DM patients than in non-DM patients[50-52]. Worse still, DM is associated with a higher risk of overall mortality in HF[53]. Although DM is a vital risk factor for HF, the effectiveness of glycemic control has not yet been proven. Some blood glucose-lowering drugs, such as insulin, thiazolidinedione (TZD), and dipeptidyl peptidase-4 (DPP-4) inhibitors, increased the risk of hospitalization for HF[54]. Therefore, the US Food and Drug Administration (FDA) requires cardiovascular outcome trials (CVOT) for all candidate drugs of DM[55]. Surprisingly, significant cardioprotective effects were demonstrated in two major trials of sodium-glucose co-transporter (SGLT) 2 inhibitors, empagliflozin (EMPA) and dapagliflozin[56, 57]. In addition, sotagliflozin (SOTA), the first reported dual SGLT1/2 inhibitor, significantly reduced the risk of HF[58]. These unexpected results of clinical studies have aroused great interest among clinical and experimental researchers.

SGLTs exist as two major isoforms; SGLT1 and SGLT2[59]. SGLT2 is explicitly expressed in the renal proximal tubule and plays a crucial role in glucose reabsorption[59, 60]. Inhibition of SGLT2 effectively reduces blood glucose by decreasing glucose reabsorption in the proximal renal tubule and increasing urine glucose excretion. Many studies have focused on the effects and mechanisms of SGLT2 inhibitors as various beneficial effects such as cardio-protection, anti-inflammation and anti-senescence have been reported[56, 61-65]. SGLT1 is expressed in small intestine and heart, contributing to glucose uptake[66]. SGLT1 in cardiomyocyte contributes to glucose uptake and plays an essential role in pathological heart conditions such as DM and ischemia[67, 68]. Inhibition of SGLT1 contributes to reducing ventricular hypertrophy and myocardial fibrosis[69].

Dual SGLT1/2 inhibitor provides a practical hypoglycemic effect by reducing glucose absorption in the small intestine and glucose reabsorption from the proximal renal tubule through SGLT1 and SGLT2 inhibition, respectively[70]. As such, SOTA provides a powerful SGLT1 inhibition effect along with an SGLT2 inhibition effect same as EMPA, so it will be able to offer an additional cardioprotective effect than EMPA. Despite the significant cardioprotective effects of these SGLT inhibitors, it has not yet

been determined whether EMPA or SOTA provide more effective cardiovascular protection.

Although the pharmacological mechanism of the glucose-lowering effect of SGLT inhibitors is well understood, the exact mechanism of cardiovascular protection is not yet clearly understood. Several recent studies have focused on sodium-hydrogen exchanger 1 (NHE1) of the myocardium as an off-target of SGLT2 inhibitors[71-73]. NHE1 is a transporter that exchanges $H^+$ and $Na^+$ and maintains intracellular pH homeostasis. NHE1 expression and activation are increased by DM-related stimuli such as hyperglycemia and insulin[74, 75], contributing to retinopathy and atherosclerosis associated with vascular abnormalities in diabetes and organ dysfunction and damage[76, 77]. Upregulation of NHE1 is also found in ventricular tissue of patients with HF[78], and experimental HF models showed that selective inhibition of NHE1 improves cardiac function by suppressing fibrosis and hypertrophy[79, 80]. These reports suggest that NHE1 plays an essential role in the pathogenesis of DM-HF. However, it has not yet been confirmed whether SOTA can target NHE1 same as other SGLT2 inhibitors, such as EMPA, and the experimental evidence to determine whether NHE1 is involved in the mechanism of cardioprotective effect is still insufficient.

In the last decade, zebrafish (*Danio rerio*) have been proposed as an excellent vertebrate animal model owing to their high fertility, cost-effectiveness, and physiological similarity to humans[81, 82]. Particularly, the pancreatic $\beta$-cells and the heart, which are essential organs for DM-HF research, are structurally and genetically similar to those of humans[83, 84]. Additionally, owing to the rapid development of zebrafish, these organs fully develop within 2–3 days post fertilization (dpf); hence, research can be conducted in a short period. Moreover, compared to other vertebrate models, which die immediately when the oxygen supply is stopped, zebrafish can survive for several hours via passive oxygen diffusion, even when blood circulation is blocked. Therefore, zebrafish larvae are widely used in cardiovascular defect studies[85]. In zebrafish larvae, which have transparent bodies, cells and organs can be directly observed under a microscope. As heart is a continuously beating organ, it is necessary to observe its contraction to accurately evaluate its function. The beating hearts of live zebrafish larvae can be directly observed via fluorescence microscopy using a transgenic (*Tg*) zebrafish line expressing the fluorescent protein in the myocardium[86]. Therefore, research using zebrafish larvae can provide information that can be easily missed while

using the existing vertebrate models.

Here, I developed DM combined with HF with reduced ejection fraction (DM-HFrEF) zebrafish larvae model[87] and evaluated the effects of EMPA and SOTA in the zebrafish model. I evaluated the role of NHE1 inhibition in the action of the two drugs.

# Materials and methods

## Zebrafish maintenance

Adult zebrafish (*Danio rerio*) were maintained at 26-28℃ on a 14/10 hours light-dark cycle in an automatic circulating tank system (Genomic Design, Daejeon, Korea). Zebrafish embryos were raised in egg water prepared by dissolving 60 μg/mL ocean salts (Sigma-Aldrich, St. Louis, MO, USA) in autoclaved deionized distilled water (DDW) at pH 7.0. Zebrafish embryos were euthanized via the low-temperature shock method when the survival rate at 24 hours post fertilization was less than 80%[88]. All experiments were performed from 3 dpf of hatched zebrafish embryos to 9 dpf. During treatment with GLU (Sigma-Aldrich, St. Louis, MO, USA), the environmental GLU solution was replaced daily to avoid contamination. I used *Tg* (*myl7:EGFP*) zebrafish expressing an enhanced green fluorescent protein (EGFP) in cardiac myosin light chain 7 (myl7)[86], and *Tg* (*ins:EGFP*) zebrafish expressing EGFP in pancreatic β-cells[89]. The Zebrafish Center for Disease Modeling (ZCDM), Korea, provided all *Tg* zebrafish. All animal experiments and husbandry procedures were approved by the Institutional Animal Care and Use Committee (IACUC) of the Seoul National University (SNU-

200310-1). Zebrafish larvae were euthanized by the hypothermic shock method exposing to ice-cold water for at least 20 min in accordance with American Veterinary Medical Association (AVMA) guidelines[90].

### Glucose colorimetric assay

As zebrafish larvae are small, the samples not sufficient to measure blood glucose levels using conventional methods. Therefore, I used an alternative method of measuring glucose in whole-body fluids. Briefly, ten larvae were transferred to a 1.5 mL tube and euthanized using the low-temperature shock method. Zebrafish larvae were gently rinsed twice with phosphate-buffered saline (PBS) and homogenized in 100 μL DDW using TissueLyser II (Qiagen, Hilden, Germany). The homogenate was then centrifuged at 13,000 rpm and 4° C for 15 minutes to obtain an eluate containing free glucose. Then, 50 μL of the eluted solution was placed in a 96-well plate and allowed to react with 50 μL of the Amplex Red reagent/HRP/glucose oxidase mixed solution, provided in the AmplexTM Red Glucose/Glucose Oxidase Assay Kit (Thermo Fisher Scientific, Waltham, MA, USA), for 30 minutes at room temperature. The absorbance was measured using a microplate reader (VERSAmax; Molecular Devices, San Jose, CA, USA) at an

excitation wavelength of 530–560 nm.

### Quantitative real-time polymerase chain reaction (qRT-PCR)

For qRT-PCR analysis, total cellular RNA was extracted from ten washed larvae using QIAzol Lysis Reagent (Qiagen, Hilden, Germany). The extracted RNA was reverse-transcribed using the amfiRivert cDNA Synthesis Premix (GenDEPOT, Katy, TX, USA) according to the manufacturer's instructions. qRT-PCR was performed using cDNA as the template, a SYBR Green PCR kit (GenDEPOT, Katy, TX, USA), and the StepOnePlus Real-Time PCR System (Applied Biosystems, Waltham, MA, USA). The expression of all genes was normalized to that of the housekeeping gene *18S ribosomal RNA* (*18s rRNA*) using the $2^{-ddCt}$ method. The primers used were as follows: *ins* (forward: 5′ -AGT GTA AGC ACT AAC CCA GGC ACA-3′ , reverse: 5′ -TGC AAA GTC AGC CAC CTC AGT TTC-3′ ), *pck1* (forward: 5′ -GAG AAT TCT CAC ACA CAC ACA CGT GAG CAG TA-3′ , reverse: 5′ -GTA AAA GCT TTC CGC CAT AAC ATC TCC AGC AGA A-3′ ), *nppb* (forward: 5′ -CAT GGG TGT TTT AAA GTT TCT CC-3′ , reverse: 5′ -CTT CAA TAT TTG CCG CCT TTA C-3′ ), *Ucn3* (forward: 5′ -GAG TGC AGG GCA GAA CAA TGT-3′ , reverse: 5′ -GAA ACT GGT TGC GCA AAG GA-3′ ), *Slc30a8* (forward:

5′ -ATC GTC TTG ATG GAA GGC AC -3′ , reverse: 5′ -TTT CTC GAA GCA CCT CCT GT -3′ ), and *18s rRNA* primers (forward: 5′ -TCG CTA GTT GGC ATC GTT TAT G-3′ , reverse: 5′ -CGG AGG TTC GAA GAC GAT CA-3′ ).

### Insulin enzyme-linked immunosorbent assay (ELISA)

As with the glucose colorimetric assay above, zebrafish larvae are small and contain very little body fluid, so there are not enough samples to measure circulating or blood insulin levels. Therefore, I measured insulin by homogenizing the whole body of 30 zebrafish larvae per sample. Insulin contents were measured with a Fish Insulin (INS) ELISA kit (MyBioSource, San Diego, CA, USA) according to the manufacturer's protocol. The absorbance was measured using a microplate reader (Infinite 200 PRO; Tecan, Männedorf, Switzerland) at an excitation wavelength of 450 nm.

### Cardiac morphology and ventricular contractility

Cardiac contractility was estimated as the ventricular fractional shortening (vFS). The *Tg* (*myl7:EGFP*) zebrafish larvae were anesthetized with 0.02% tricaine (MS222, Sigma-Aldrich, St. Louis, MO, USA) and then embedded in 3% methylcellulose (Sigma-Aldrich, St. Louis, MO, USA). The beating heart was observed using

an automated inverted fluorescence microscope (Leica DMI6000B; Leica Microsystems, Wetzlar, Germany). The heart of individual zebrafish larva was imaged continuously for 30 s. The vFS was calculated using the ventricular dimension at the end-systole ($VD_s$) and end-diastole ($VD_d$). Calculation formula is as follows:

$$vFS = (VD_d - VD_s) / VD_d \times 100$$

### Measurement of blood flow-based cardiac contraction irregularity

Cardiac contraction irregularity was estimated as the standard deviation (SD) of the beat-to-beat interval. Zebrafish larvae anesthetized with 0.02% tricaine were embedded in 3% methylcellulose and positioned such that the dorsal aorta was visible. Blood flow was recorded for 30 s using a high-speed camera and the ZebraBlood of the MicroZebraLab system (ViewPoint, Civrieux, France). Subsequently, real-time blood flow pulses were analyzed using ZebraBlood. The blood flow data were used to identify peaks using the FindPeaks function of MATLAB (MathWorks, Natick, MA, USA), and the time between the peaks was calculated to determine the beat-to-beat interval. MATLAB was used to set an appropriate threshold to identify the correct peaks.

### Motility test and survival analysis

Zebrafish larvae motility was analyzed using DanioVision and EthoVision XT (Noldus, Wageningen, Netherlands). Zebrafish larvae were individually placed in square 96-well plates containing 200 μL egg water, and movements were tracked and recorded for 5 minutes using DanioVision. While monitoring zebrafish larvae motility, they were stimulated with a tapping device once every 30 seconds. Zebrafish motility analysis using EthoVision XT included the assessment of movement distance, velocity, acceleration, and duration. Kaplan-Meier survival analysis was used for survival analysis. Each zebrafish was transferred to a 96-well plate containing 200 μL egg water. Survival was observed using a microscope every 12 hours until 9 dpf.

### *In silico* molecular docking analysis

A protein structure prediction model of zebrafish NHE1 was prepared using an AlphaFold Protein Structure Database developed by DeepMind (London, UK) and European Bioinformatics Institute (EMBL-EBI, Cambridgeshire, UK) [91]. The 3D structures of GLU, EMPA, SOTA, and Cariporide (CARI) for molecular docking analysis were obtained from PubChem. The binding sites and energy of ligands binding to zebrafish NHE1 were analyzed using

AutoDock Vina[92]. All molecular docking analysis results were visualized using PyMOl (Schrödinger, New York, NY, USA).

### Drug affinity responsive target stability (DARTS)

DARTS assay is an experimental method for identifying and studying protein-ligand interactions[93]. I performed a DARTS assay to demonstrate the binding of SGLTs inhibitors to zebrafish NHE1 experimentally. More than 500 zebrafish larvae were anesthetized with tricaine and then euthanized by cold shock. To separate zebrafish tissues into single cells, they were reacted with 0.2% trypsin EDTA and collagenase[94]. After washing the separated cell lysate twice, the protein was extracted by mildly lysing the cells using M-PER (Thermo Fisher Scientific, Waltham, MA, USA). The amount of protein was quantified through BCA Protein assay (Thermo Fisher Scientific, Waltham, MA, USA), and DMSO, EMPA, SOTA, or CARI (Sigma-Aldrich, St. Louis, MO, USA, St. Louis, MO, USA) was reacted at RT for 1 hour. After that, pronase (Sigma-Aldrich, St. Louis, MO, USA) was reacted for 30 minutes, and SDS-PAGE was performed. Then, it was transferred to polyvinylidene difluoride membranes (PVDF, Merck Millipore, Darmstadt, Germany) and blocked with 5% skim milk for one hour at room temperature. The membrane was incubated with antibodies

of NHE1 (Thermo Fisher Scientific, Waltham, MA, USA) and GAPDH (Abcam, Cambridge, UK) overnight at 4° C. Anti-Rabbit secondary antibody (GenDEPOT, Katy, TX, USA) was incubated for one hour at room temperature and then detected using Amersham Imager 600 (GE Healthcare, Chicago, IL, USA).

### Measurement of intracellular $H^+$, $Na^+$ and $Ca^{2+}$ concentration

To measurement of intracellular $H^+$, $Na^+$ and $Ca^{2+}$ concentrations, I used the Rat H9C2 cardiomyocytes cultured with 10% fetal bovine serum (FBS) with Dulbecco Modified Eagle Medium (DMEM, GenDEPOT, Katy, TX, USA) in 96 well black plates (Corning, New York, USA), The H9C2 cells are incubated with/without adding 40 mM D-glucose solution for 24 hours after replacement with low glucose DMEM (GenDEPOT, Katy, TX, USA). After treatment with EMPA, SOTA, or CARI for 2 or 24 hours, staining for intracellular ion measurement was performed. Staining of $H^+$, $Na^+$ or $Ca^{2+}$ was performed using pHrodo Red AM (Thermo Fisher Scientific, Waltham, MA, USA), SBFI AM (Abcam, Cambridge, UK) or Fluo-4 AM (Thermo Fisher Scientific, Waltham, MA, USA), respectively, and was performed according to the respective manufacturer's instructions. Briefly, all staining were performed using live cell imaging solution (LCIS, Thermo Fisher Scientific, Waltham, MA,

USA) containing HEPES. After washing with LCIS, cultured cells were incubated at 37° C for 30 minutes with pHrodo Red AM or Fluo-4 AM or 60 minutes in SBFI AM. After staining with pHrodo Red AM, SBFI AM or Fluo-4 AM, fluorescence at 560/580 nm, 340/500 nm and 494/516 nm, respectively, was measured using a SPARK multimode microplate reader (TECAN, Männedorf, Switzerland).

### Statistical analysis

All data are presented as mean ± SD. Statistical analyses were performed with GraphPad Prism 8 (GraphPad Software, San Diego, CA, USA). Data were analyzed using the Student's t-test or Mann-Whitney U-test to compare two groups, or a one-way analysis of variance (ANOVA) followed by the Tukey post-hoc test for compare more than two groups. The Kaplan-Meier method with the Log-rank test was used for survival analysis.

# Results

## Effects of concentrations of D-glucose and/or Streptozotocin on the survival rates in zebrafish larvae.

To use the DM zebrafish model for experiments, the baseline survival rate must be stabilized; however, GLU is toxic and can affect survival. Therefore, I evaluated the viability of zebrafish larvae treated with different concentrations of GLU. Because of GLU treatment from 3 to 9 dpf (Figure 1A), immersion in 60-100 mM GLU for over 48 hours had lethal effects on zebrafish larvae, resulting in a sharp decrease in their survival rates (Figure 1B). However, no significant reduction in viability was observed after immersion in GLU concentrations 20 and 40 mM (Figure 1B). Viability was assessed in the presence of 40 mM GLU and various concentrations of STZ (Figure 1A). A high STZ concentration (100, 200 and 300 $\mu$g/mL) significantly reduced the survival rate, whereas 50 $\mu$g/mL STZ treatment did not affect the survival rate (Figure 1C).

## Induction of hyperglycemia and impairment of glucose homeostasis in zebrafish model with the combination of D-glucose and Streptozotocin (GLU/STZ)

DM is characterized by hyperglycemia and impaired glucose homeostasis owing to abnormal insulin expression or function. Therefore, I measured whole-body glucose concentration as an alternative blood glucose measurement parameter in zebrafish larvae. The GLU/STZ treatment resulted in a significant increase in whole-body glucose concentration compared with that in the control (Figure 2A). The GLU-only group also increased whole-body glucose concentrations, but not as high as GLU/STZ (Figure 2A). Additionally, after the high-glucose challenge, whole-body glucose levels in the GLU/STZ group stabilized more slowly than those in the control group and showed a tendency to fluctuate (Figure 2B and C). I then confirmed the expression of insulin and phosphoenolpyruvate carboxykinase (PEPCK), an essential enzyme involved in gluconeogenesis, in zebrafish treated with GLU/STZ. The same concentration D-mannitol (MAN) was used as an osmotic control for GLU. The expression of *ins*, a preproinsulin gene, was significantly higher in the GLU-only group than in the control and MAN groups. In contrast, the expression of *ins* in the GLU/STZ-treated zebrafish was completely suppressed (Figure 3A). This has also been observed in whole-body insulin contents (Figure 3C). Additionally, the expression of *pck1*, a PEPCK gene, showed a statistically significant increase in the GLU/STZ group

compared to that in other groups, but there was no change in its expression in the GLU or MAN groups (Figure 3B).

Despite the GLU/STZ-induced hyperglycemia and glucose homeostasis abnormalities, no change was observed in the morphology of pancreatic β-cells of zebrafish larvae (Figure 3F). Also, there was no significant change in the gene expression of *ucn3* and *slc30a8*, markers of mature pancreatic β-cells (Figure 3D and E). Based on these results, zebrafish treated with GLU/STZ was called DM zebrafish below.

## Establishment of heart failure with reduced contractility via consecutive treatment with Terfenadine post diabetes mellitus induction

HF with reduced ejection fraction is mainly characterized by reduced cardiac contractility and increased irregular contractions. Therefore, I evaluated cardiac contractility and irregular contraction after treatment with Terfenadine (TER), cardiotoxic potassium channel blocker, in DM or non-DM zebrafish. First, the hearts of *Tg* (*myl7:EGFP*) zebrafish were observed under a fluorescence microscope, and then the ventricle contraction was evaluated (Figure 4A). The vFS was not reduced in the DM zebrafish model; however, TER treatment in non-DM zebrafish slightly reduced the

vFS compared with that in the control. Importantly, TER-treated DM zebrafish showed a remarkable reduction in the vFS compared with non-DM zebrafish treated with the same TER concentration (Figure 4A and B). Next, contraction irregularity was evaluated via blood flow analysis. Irregular contractions were observed in both the groups treated with TER but not in the non-DM and DM groups (Figure 5A). Particularly, severe irregular contractions were observed in the TER-treated DM zebrafish (Figure 5A). The SD of the beat-to-beat interval, indicating irregular cardiac contractions, was significantly higher in the TER-treated DM zebrafish than in the TER-treated non-DM zebrafish (Figure 5B). Additionally, the expression of *nppb*, the gene encoding natriuretic peptide B, an HF biomarker, was also significantly increased in TER-treated DM zebrafish compared to that in other groups (Figure 5C).

### Evaluation of global motility and viability in Terfenadine treated-diabetes mellitus zebrafish model

After 24 hours of treatment of non-DM and DM zebrafish with TER, each zebrafish was tracked to evaluate motility (Figure 6A). TER treatment reduced the distance moved and movement duration in both the non-DM and DM groups (Figure 6A-C). Particularly, the TER-treated DM zebrafish demonstrated markedly reduced moved

distance compared to the other groups, and the distance moved of TER-treated DM zebrafish was significantly lower than that of the TER-treated non-DM zebrafish (Figure 6B). However, no statistical difference was observed between TER-treated non-DM and TER-treated DM zebrafish in terms of the movement duration. (Figure 6C). The survival rate showed a tendency similar to that of motility. Furthermore, a reduction in the survival rate was observed in the TER-treated non-DM zebrafish. However, the survival rates of TER-treated DM zebrafish decreased more remarkable than those of other groups (Figure 6D). Based on these results, the DM zebrafish model with reduced ejection fraction by treatment with TER was called DM-HFrEF zebrafish below.

### Treatment with Empagliflozin or Sotagliflozin improves survival and motility in DM-HFrEF zebrafish.

I observed the effect of different concentrations of EMPA or SOTA in DM-HFrEF zebrafish model. I first observed the viability of DM-HFrEF zebrafish after treatment with various concentrations of EMPA or SOTA to determine whether EMPA or SOTA increased the survival rate of the DM-HFrEF zebrafish model (Figure 7). The DM-HFrEF model significantly reduced 8 and 9 dpf survival, whereas the treatment with 0.2, 1, and 5 $\mu$M of EMPA (Figure 7 A

and C) or SOTA (Figure 7B and D) significantly increased 8 and 9 dpf survival of DM-HFrEF zebrafish model (Figure 7A-D). Interestingly, a significant increase was observed with 25 μM of EMPA (Figure 7A and C), but SOTA at the same concentration did not (Figure 7B and D).

Next, I evaluated the changes in the motility of DM-HFrEF zebrafish with various concentrations of EMPA or SOTA treatment (Figure 8). Either EMPA or SOTA treatment significantly preserved the motility of the DM-HFrEF zebrafish model (Figure 8A-C). In particular, 1 and 5 μM of EMPA or SOTA significantly improved the movement distance of DM-HFrEF zebrafish. On the other hand, in DM-HFrEF zebrafish treated with 0.2 μM of EMPA or 0.2 and 25 μM SOTA, no significant increase in movement distance was observed. (Figure 8B). Movement duration also showed a similar trend. A significant increase was observed in the treatment groups of 1, 5 and 25 μM of EMPA or 1 and 5 μM of SOTA, whereas no significant difference was observed between 0.2 μM of EMPA and 0.2 and 25 μM of SOTA group. (Figure 8C).

**Changes in morphology according to the concentration of empagliflozin or sotagliflozin treatment in the DM-HFrEF zebrafish**

model

When I evaluated the gross morphology, no significant difference in morphology was observed between the groups, regardless of DM or HF status (Figure 9A-D). In addition, morphological abnormalities were not observed in DM-HFrEF zebrafish treated with 0.2, 1, 5 and 25 μM EMPA or 0.2, 1 and 5 μM SOTA (Figure 9E-H). Epicardial edema was observed in zebrafish larvae treated with 25 μM SOTA, and interestingly a marked uninflated swim bladder was observed in these compared to other groups (Figure 9L and M). The uninflated swim bladder caused by the high molarity of SOTA was observed not only in DM-HFrEF zebrafish model but also in the HF induced non-DM zebrafish (Figure 10A and B).

Treatment with empagliflozin or sotagliflozin improved cardiac functions in the DM-HF zebrafish model.

According to clinical studies, EMPA and SOTA has been confirmed to have a significant protective effect on DM-HFrEF, but the effects of the two drugs have not been compared. Therefore, I compared the cardiac effects of EMPA with those of SOTA. Either EMPA or SOTA treatment preserved contractile function in the DM-HFrEF zebrafish model, in which a marked decrease in cardiac function was observed compared to non-DM or DM-only models

(Figure 10).

Ventricular contractility is estimated by the vFS parameter. There was no difference in vFS between non-DM and DM-only zebrafish, but a significant decrease in vFS was observed in DM-HFrEF zebrafish compared to DM-only zebrafish (Figure 11A and B). Treatment with EMPA or SOTA significantly enhanced the vFS of DM-HFrEF zebrafish at various concentrations. Treatment with 0.2-5 $\mu$M of both drugs significantly improved vFS, although no significant change was observed at 0.04 $\mu$M (Figure 11A and B). Notably, the vFS preservation effect of EMPA peaked at 5 $\mu$M, whereas SOTA peaked at 1 $\mu$M (Figure 11B). There was also no significant difference between groups in terms of heart morphology (Figure 11A).

The heart is a regular and constantly beating organ, and irregular contraction is a hallmarks of HF. The SD of beat-to-beat intervals was calculated to quantify irregular contractions. In DM-HFrEF zebrafish, more irregular contractions were observed compared to the non-DM or DM-only group. A marked increase in the SD of the beat-to-beat interval was mainly observed in the DM-HFrEF zebrafish (Figure 10C and D). The SD of the beat-to-beat interval in the DM-HFrEF zebrafish treated with 0.2-5 $\mu$M EMPA or SOTA was significantly preserved, but not

0.04 μM EMPA or SOTA treatment (Figure 12A and B).

In addition, the *nppb*, a gene of the zebrafish form of the B-type natriuretic peptide, a biomarker of HF, was markedly increased in DM-HFrEF zebrafish, whereas it was significantly decreased in both EMPA and SOTA-treated groups (Figure 13A). EMPA and SOTA treatments did not affect expression of *ins*, a preproinsulin gene, and *pck1*, a phosphoenolpyruvate carboxykinase (PEPCK) 1 gene involved in gluconeogenesis, unlike the improvement in survival rate, motility, and cardiac function (Figure 13B and C).

**Both EMPA and SOTA bind structurally to zebrafish NHE1 and inhibit its function.**

Since several studies have recently reported evidence that SGLT2 inhibitors, including EMPA, can inhibit NHE1[71-73], I sought to determine the effects of EMPA and SOTA on NHE1 in zebrafish. First, I performed *in silico* analysis of EMPA and SOTA binding to the structural prediction model of NHE1. As a result, EMPA, SOTA, and Cariporide (CARI), a selective inhibitor of NHE1, were bound to the same site in zebrafish NHE1 (Figure 14A). In addition, the binding affinity of EMPA, SOTA and CARI was -7.8, -7.2 and -6.1 kcal/mol, respectively, which were higher than the negative control GLU (-4.7 kcal/mol, Figure 14B).

I then compared the binding of EMPA and SOTA to zebrafish NHE1 by drug affinity responsive target stability (DARTS) assay *in vitro* (Figure 15A). Pronase treatment resulted in rapid proteolytic degradation of NHE1 in VEH-treated zebrafish proteins, whereas proteolytic protection was observed in zebrafish proteins treated with EMPA, SOTA or CARI (Figures 15B). The NHE1 band intensity of the groups treated with EMPA, SOTA, or CARI was statistically significantly higher than that of the VEH group (Figure 15B and C). However, GAPDH used as a loading control was consistently proteolysis by pronase regardless of treatment with EMPA, SOTA, or CARI (Figure 15B and D).

Lastly, I confirmed the functional inhibition of NHE1 by EMPA and SOTA in vitro. Activation of NHE1 exchanges intracellular $H^+$ with extracellular $Na^+$, and influxed $Na^+$ is again exchanged with $Ca^{2+}$ through sodium-calcium exchanger (NCX), resulting in an increase in intracellular pH, $Na^+$, and $Ca^{2+}$[79]. I evaluated whether these ion concentrations were changed by EMPA or SOTA in cardiomyocytes under high glucose (HG) conditions. In HG, intracellular $Na^+$ and $Ca^{2+}$ were increased compared to low glucose (LG) conditions, but treatment with EMPA, SOTA or CARI suppressed the change in the intracellular $Na^+$ and $Ca^{2+}$

concentrations caused by HG (Figure 16A and B). Similarly, treatment with EMPA, SOTA or CARI suppressed the slight concentration change of intracellular $H^+$ mediated by HG but no significant difference (Figure 16C). Those reduction effects were observed at both 2 h and 24 h after EMPA, SOTA or CARI treatment (Figure 16). The inhibitory effect on changes in intracellular ions by EMPA or SOTA treatment showed a concentration-dependent tendency, and statistical significance was observed at 5 $\mu$M. In particular, the intracellular $Na^+$ concentration of cells treated with SOTA showed a significant difference at 0.04-5 $\mu$M concentration (Figure 17). Additional treatment with EMPA or SOTA after CARI treatment did not induce changes in intracellular $Ca^{2+}$, and additional treatment with EMPA did not induce changes in intracellular $Na^+$ (Figure 18A and B). On the other hand, additional treatment with SOTA induced a significant decrease in intracellular $Na^+$ than other groups (Figure 18B).

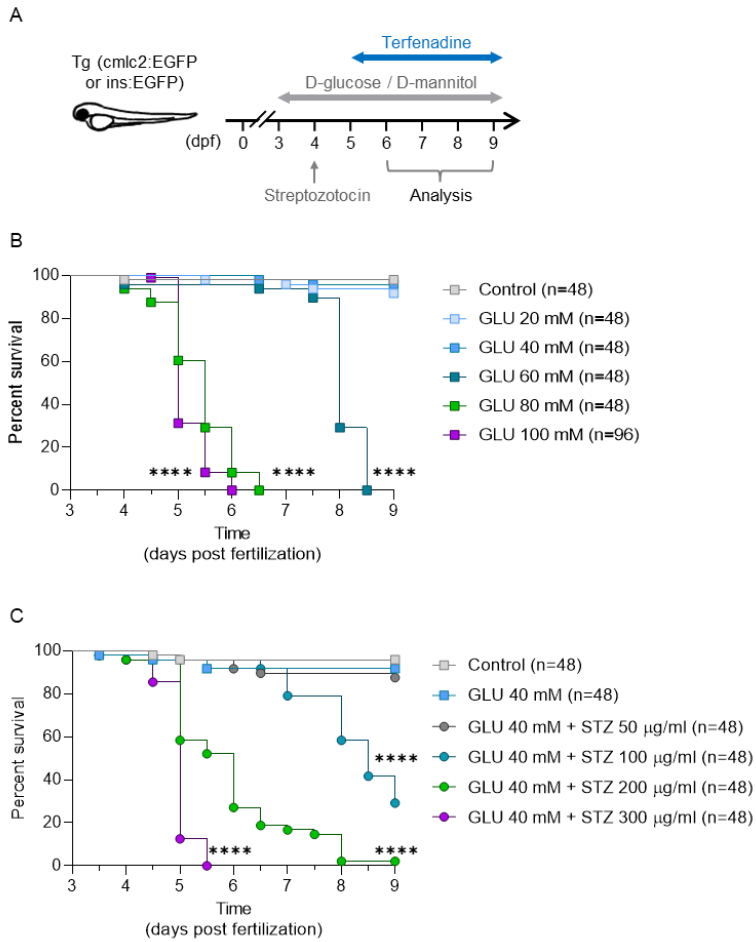


**Figure 1.** Effects of various concentrations of D-glucose and/or Streptozotocin on the survival rates and motility of zebrafish larvae. (A) Schematic of the study design. (B) Kaplan-Meier survival analysis of zebrafish larvae after treatment with various concentrations of GLU (n = 48 per group) and (C) a combination of 40 mM GLU and various concentrations of STZ. (n = 48 per group) ****$p < 0.0001$ vs. (B) control group or (C) GLU 40 mM group.

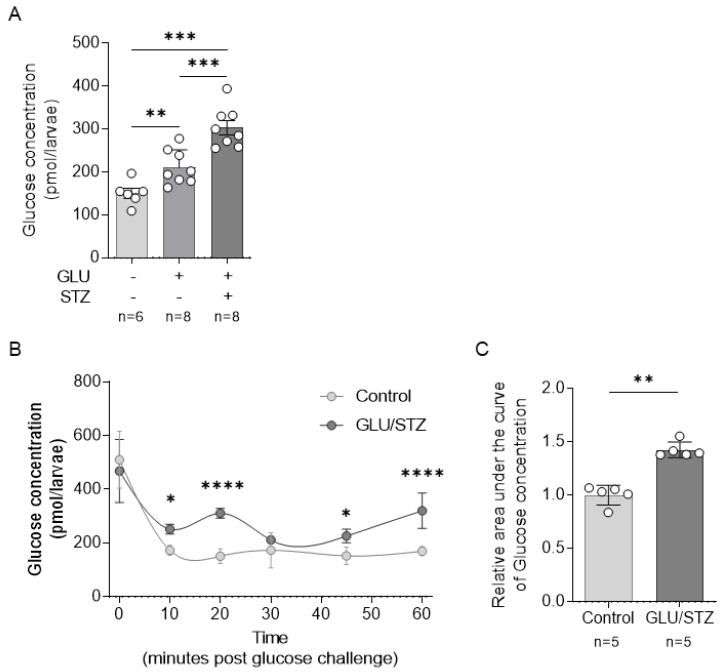


**Figure 2.** Induction of hyperglycemia in zebrafish larvae via combined treatment with D-glucose and Streptozotocin. (A) Whole-body glucose concentration (n = 6-8 per group). (B) Changes in whole-body glucose concentration after high-GLU challenge and (C) the corresponding area under the curve (AUC) (n = 5 per group). Each group had 5-8 samples, with 10 larvae per sample. Data are presented as mean ± standard deviation and each dot represents the value of each sample. $*p < 0.05$, $**p < 0.01$, $***p < 0.001$, $****p < 0.0001$ vs. indicated group.

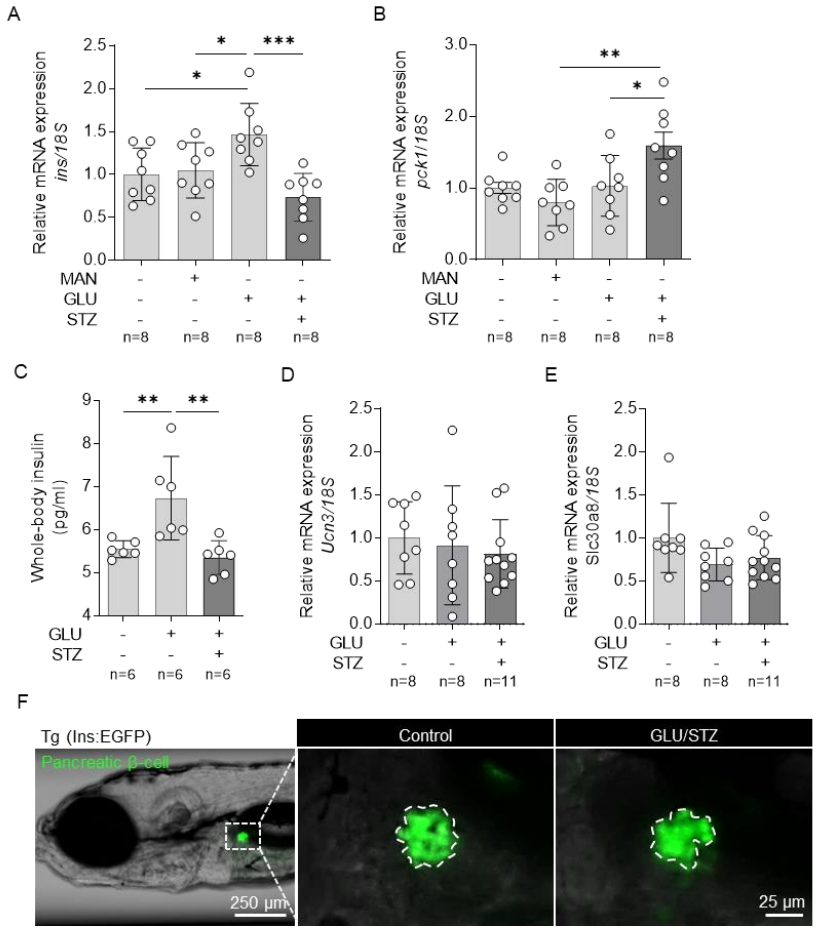


**Figure 3.** Induction of diabetes mellitus-like phenotypes in zebrafish larvae via combined treatment with D-glucose and Streptozotocin. (A) Relative mRNA expression of *ins* and (B) *pck1* (n = 8 per group). (C) Whole-body insulin level (n = 6 per group). (D) Relative gene expression of *Ucn3* and (E) *Slc30a8* (n = 8-11 per group). (F) Representative fluorescence microscopic image of pancreatic β-cells of the *Tg* (*ins:EGFP*) zebrafish larvae. Each group had 6-11 samples, with (A, B, D and E) 10 or (C) 30 larvae per sample. Data are presented as mean ± standard deviation and

each dot represents the value of each sample. $*p < 0.05$, $**p < 0.01$, $***p < 0.001$ vs. indicated group.

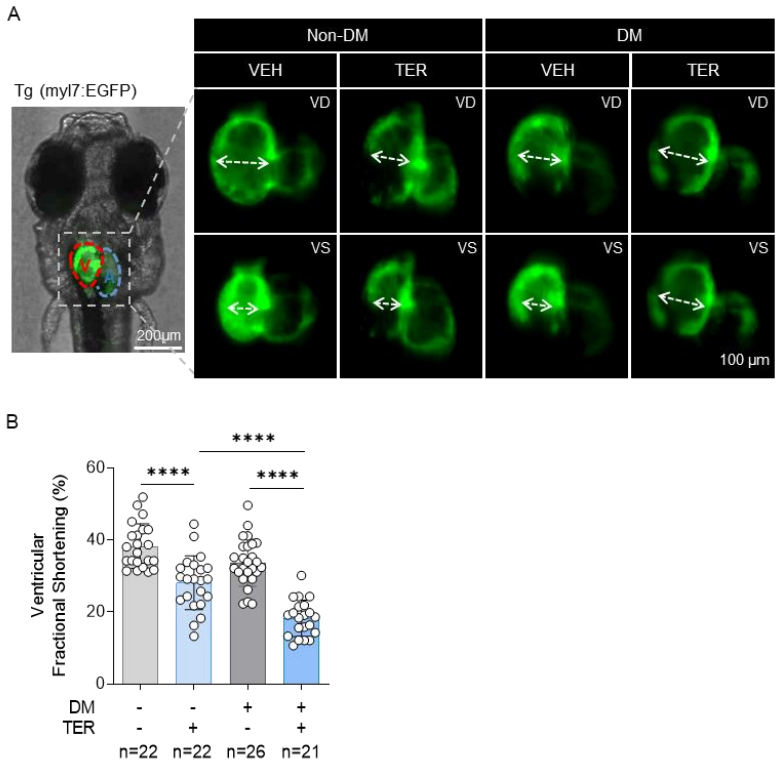


**Figure 4.** Reduced cardiac contractility by treatment with Terfenadine in the diabetes mellitus zebrafish model. (A) Representative fluorescent microscopic images of the *Tg* (*myl7:EGFP*) zebrafish heart with a green fluorescent protein (GFP) at 7 dpf. (B) Ventricular fractional shortening (vFS) (n = 21–26 per group). Data are presented as mean ± standard deviation and each dot represents the value of each zebrafish larva. ****$p$ < 0.0001 vs. indicated group.

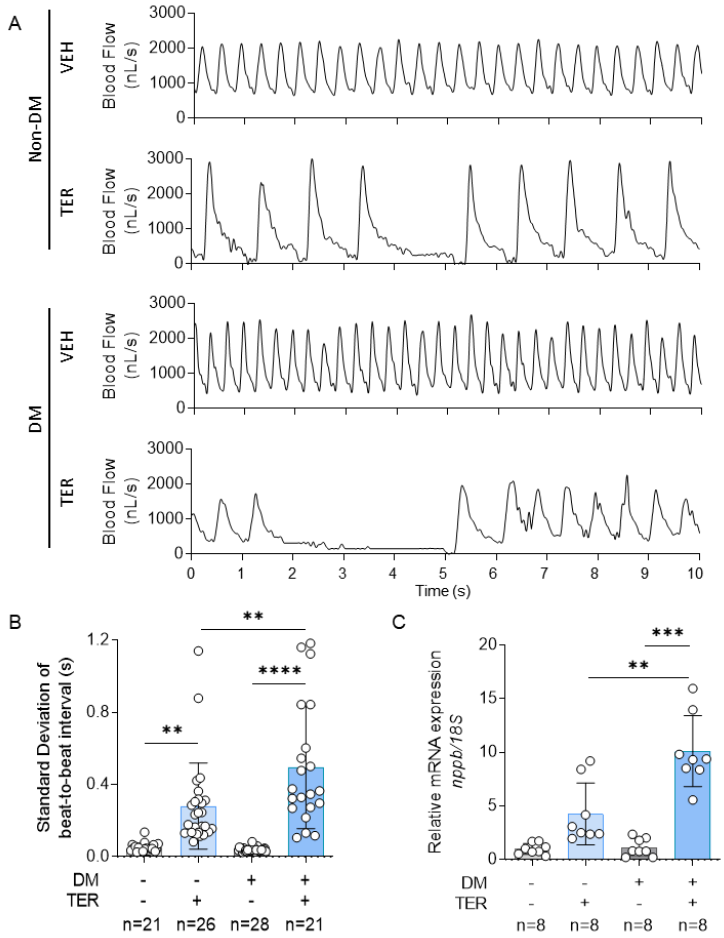


**Figure 5.** Induced irregular cardiac contraction by treatment with Terfenadine in the diabetes mellitus zebrafish model. (A) Representative blood pulse graphs. (B) Standard deviation of the beat-to-beat interval (n = 21-28 per group). (C) Relative mRNA expression of *nppb* (n = 8 per group). Each group had 8 samples, with 10 larvae per sample. Data are presented as mean ± standard deviation and each dot represents the value of each (B) zebrafish larva or (C) sample. $^{**}p < 0.01$, $^{***}p < 0.001$, $^{****}p < 0.0001$ vs. indicated group.

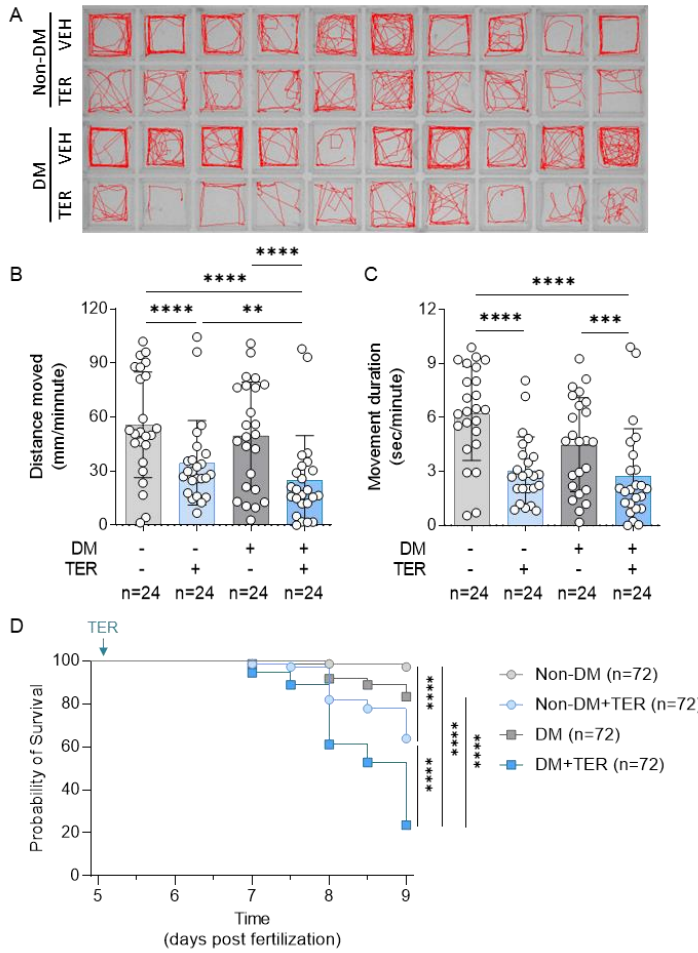


**Figure 6.** Reduced motility and viability in the Terfenadine treated-diabetes mellitus zebrafish model. (A) Representative images of motility tracking for 5 minutes in zebrafish larvae. (B) Average moved distance and (C) movement duration per minute (n = 24 per group). Data are presented as mean ± standard deviation and each dot represents the value of each zebrafish larva. (D) Kaplan-Meier survival analysis (n = 72 per group). $^{**}p < 0.01$, $^{***}p < 0.001$, $^{****}p < 0.0001$ vs. indicated group.

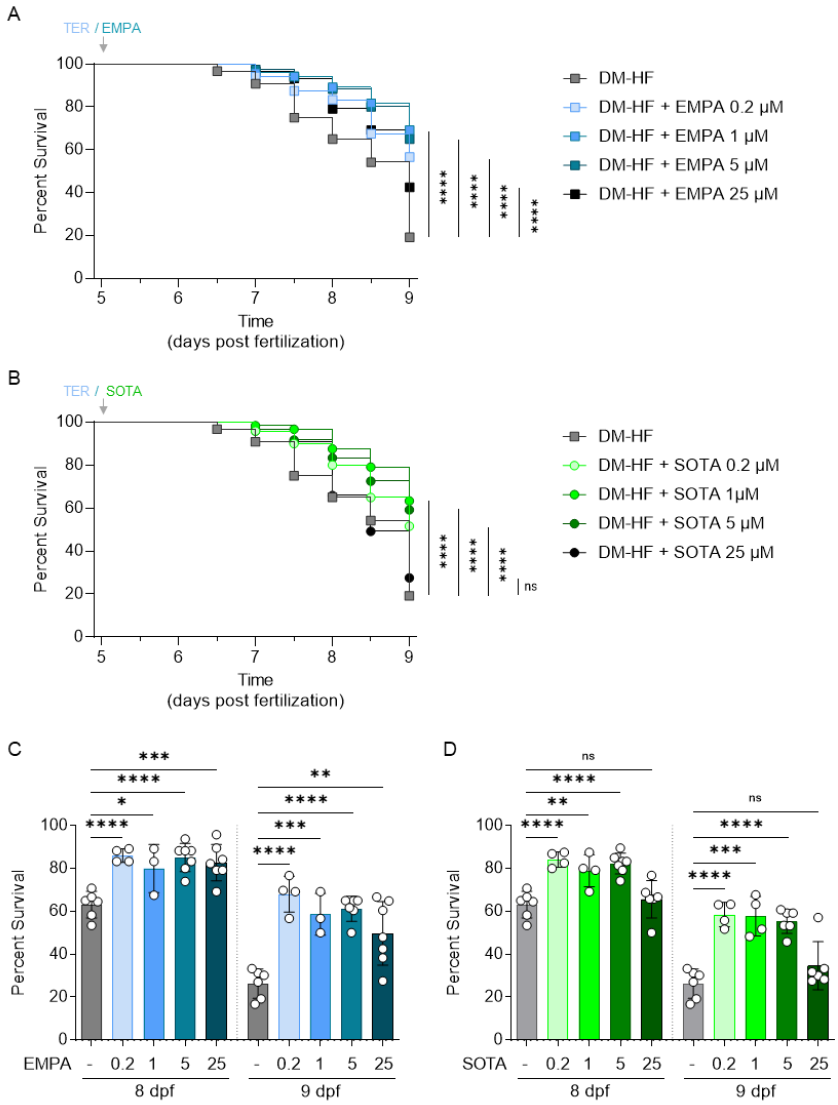


**Figure 7.** Comparison of concentration-dependent survival rates of treatment of Empagliflozin or Sotagliflozin. Kaplan-Meier survival analysis of zebrafish larvae after treatment with 0.2, 1, 5 and 25 $\mu$M of (A and B) empagliflozin or (C and D) sotagliflozin treated DM-HF zebrafish (n = 120 per group). The DM-HF group was tested under the same conditions on the same day and the graph was separated. Figure 1C and D are presented as mean ± standard

deviation and each dot represents the value of each experiment. *$p$ < 0.05, **$p$ < 0.01, ***$p$ < 0.001, ****$p$ < 0.0001 vs. indicated group.

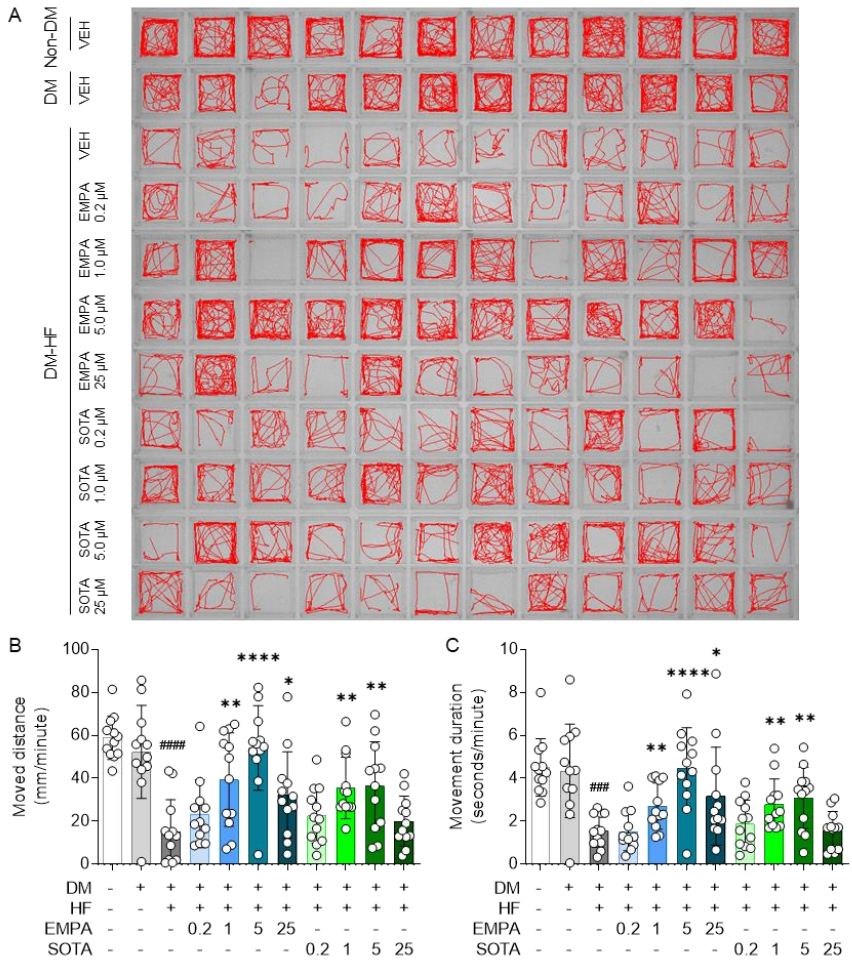


**Figure 8.** Comparison of concentration-dependent motility conservation effect of Empagliflozin or Sotagliflozin. (A) Representative motility tracking images of zebrafish larvae for 5 minutes. (B) Average moved distance and (C) movement duration per 1 minute (n = 12 per group). Data are presented as mean ± standard deviation and each dot represents the value of each zebrafish larvae. $*p < 0.05$, $**p < 0.01$, $****p < 0.0001$ vs. DM-HF group, and $^{\#\#\#}p < 0.001$, $^{\#\#\#\#}p < 0.0001$ vs. DM group.

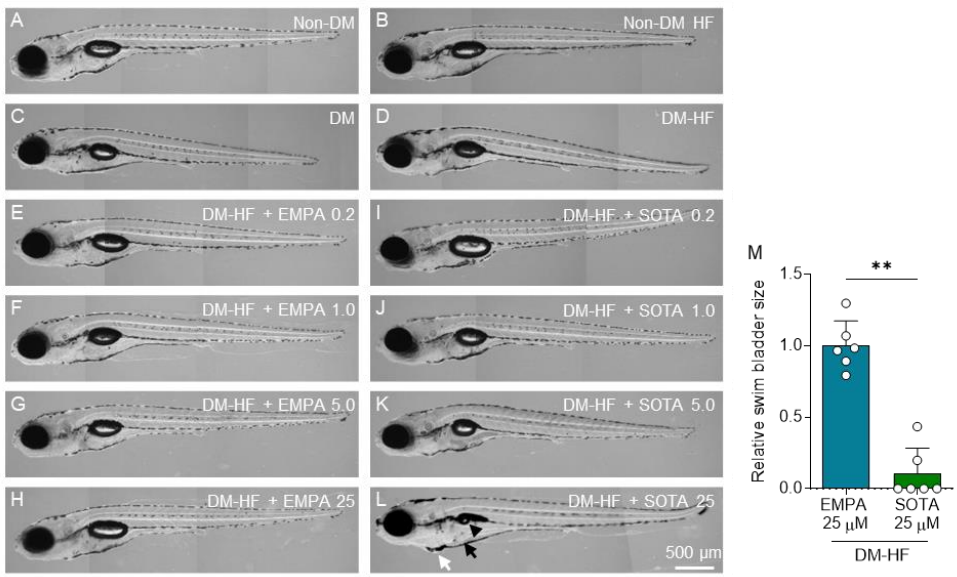


**Figure 9.** Morphology of DM-HFrEF zebrafish treated with Empagliflozin or Sotagliflozin. (A) non-DM, (B) non-DM with HFrEF, (C) DM, (D) DM-HFrEF. (E-L) DM-HFrEF zebrafish following treatment with (E) 0.2, (F) 1, (G) 5 and (H) 25 $\mu$M of Empagliflozin or (I) 0.2, (J) 1, (K) 5, and (L) 25 $\mu$M of Sotagliflozin. (M) Relative size of zebrafish swim bladder treated with 25 $\mu$M of Empagliflozin or Sotagliflozin (n = 5 per group). Data are presented as mean ± standard deviation and each dot represents the value of each zebrafish larvae. $^{**}p < 0.01$ vs. indicated group.

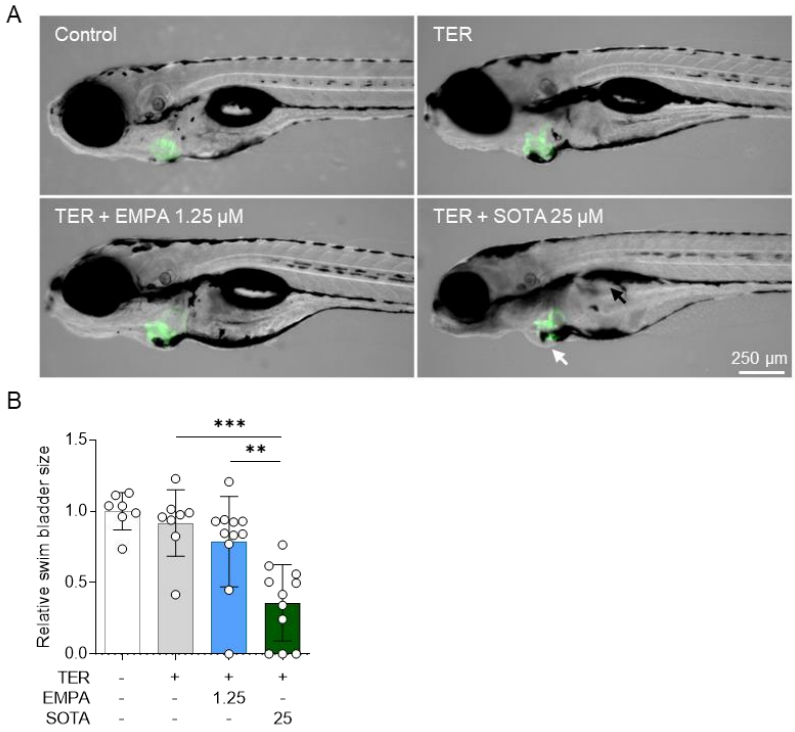


**Figure 10.** Uninflated swim bladder in high dose sotagliflozin treated HF induced non-DM zebrafish model. (A) Morphology of non-DM zebrafish with or without HF. (B) Relative size of swim bladder of HF induced non-DM zebrafish treated with 1.25 $\mu$M Empagliflozin or 25 $\mu$M Sotagliflozin (n = 11 per group). Data are presented as mean ± standard deviation and each dot represents the value of each zebrafish larvae. $^{**}p < 0.01$, $^{***}p < 0.001$ vs. indicated group.

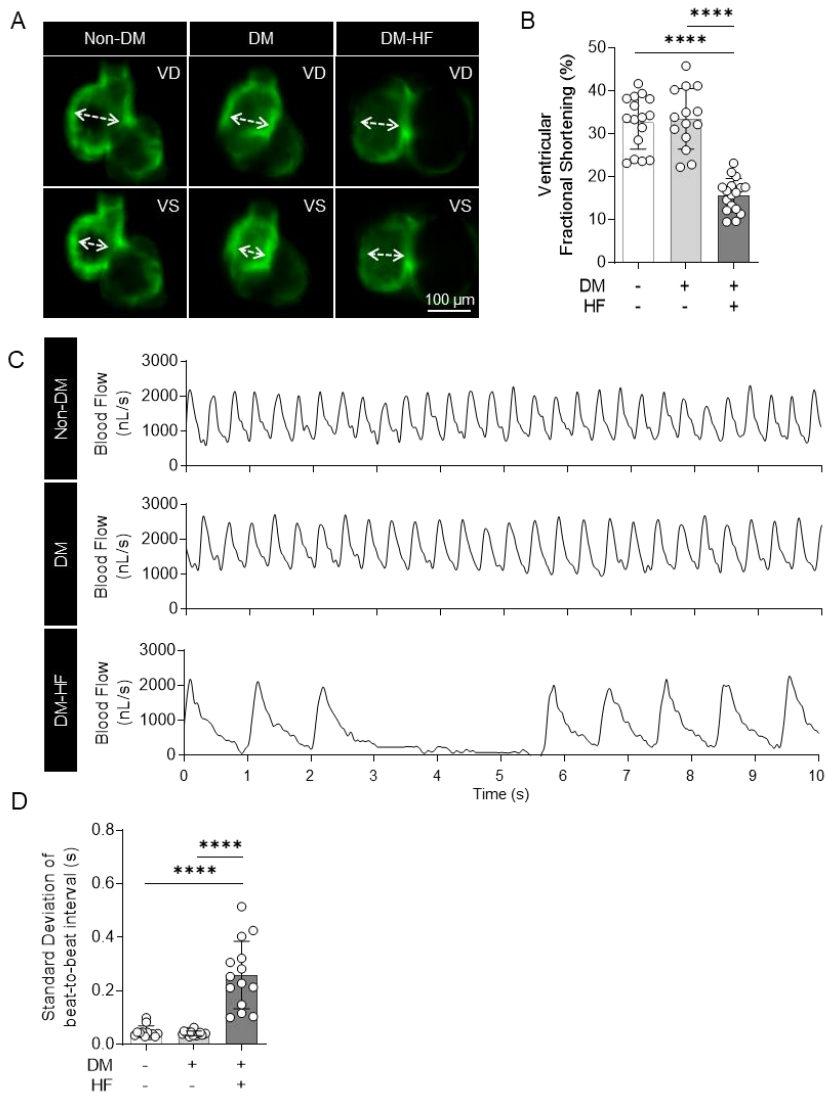


**Figure 11.** Cardiac contractile functions in the DM-HFrEF zebrafish model. (A) Representative fluorescent microscopy images of *Tg* (*myl7:EGFP*) zebrafish heart with a green fluorescent protein (GFP). (B) Ventricular fractional shortening calculated based on fluorescent images. (n=13-17 per group). (C) Representative blood flow graphs. (D) Standard deviation of beat-to-beat interval analyzed based on blood flow (n = 14-28 per group). Data are

presented as mean ± standard deviation and each dot represents the value of each zebrafish larvae. ****$p < 0.0001$ vs. indicated group.

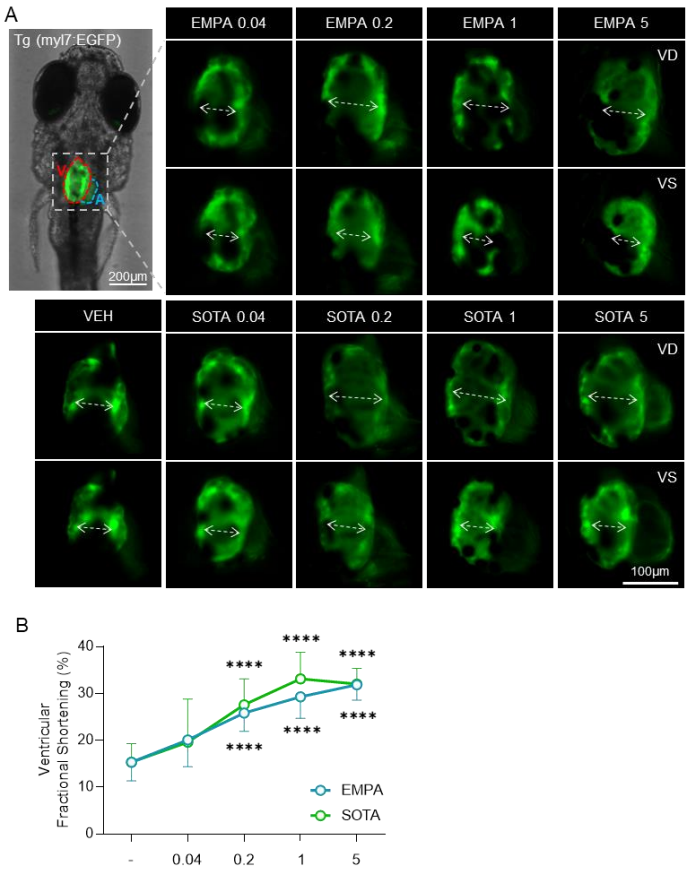


**Figure 12.** Treatment with Empagliflozin or Sotagliflozin improved cardiac contractility in the DM-HFrEF zebrafish model. (A) Representative fluorescent microscopy images of *Tg* (*myl7:EGFP*) zebrafish heart with a green fluorescent protein (GFP). (B) Ventricular fractional shortening calculated based on fluorescent images. (n=8-25 per group). Data are presented as mean ± standard deviation and each dot represents the value of each zebrafish larvae. ****$p < 0.0001$ vs. control group.

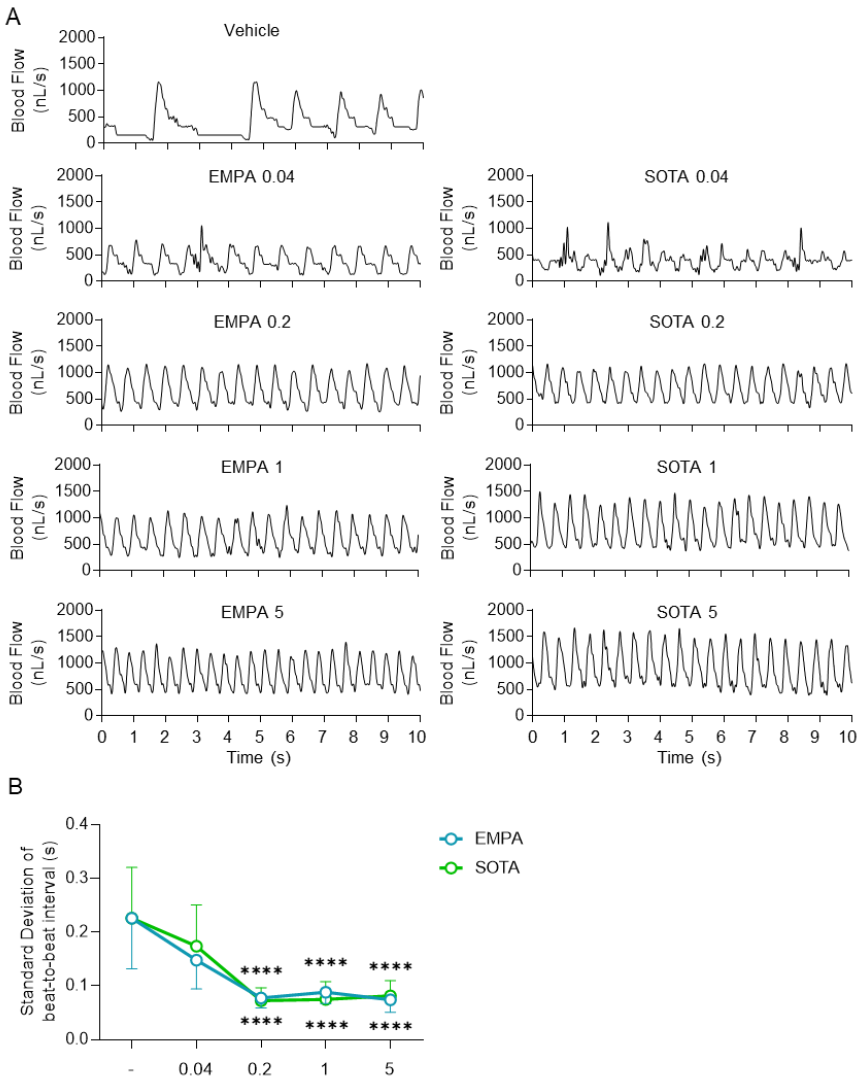


**Figure 13.** Treatment with Empagliflozin or Sotagliflozin suppress irregular contraction in the DM-HFrEF zebrafish model. (A) Representative blood flow graphs. (B) Standard deviation of beat-to-beat interval analyzed based on blood flow (n = 12-17 per group). Data are presented as mean ± standard deviation. ****$p$ < 0.0001 vs. indicated group.

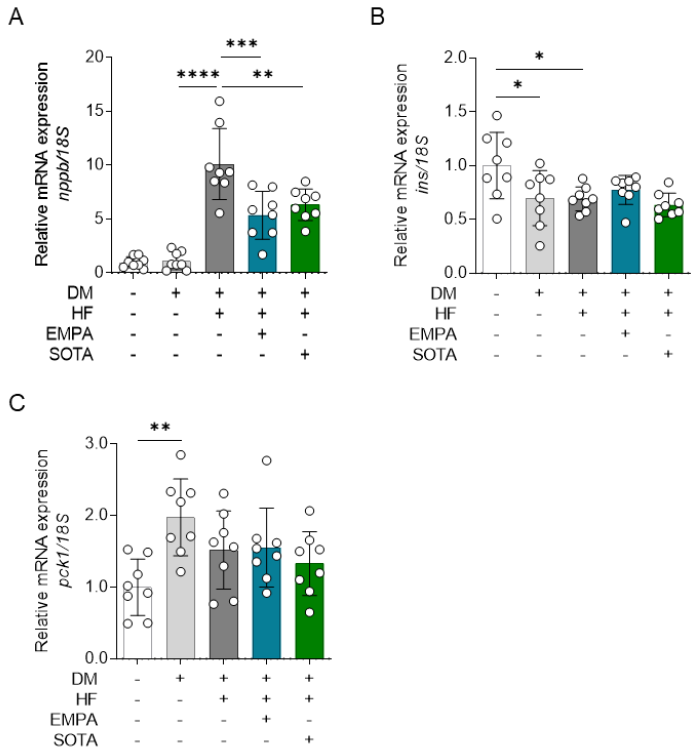


**Figure 14.** Gene expression of *nppb*, *ins* and *pck1* in the DM−HFrEF zebrafish treated with Empagliflozin or Sotagliflozin. (A) Relative mRNA expression of *nppb*, (B) *ins* and (C) *pck1* (n = 8 per group). Each group had 8 samples, with 10 larvae per sample. Data are presented as mean ± standard deviation and each dot represents the value of each sample. *$p < 0.05$, **$p < 0.01$, ***$p < 0.001$, ****$p < 0.0001$ vs. indicated group.

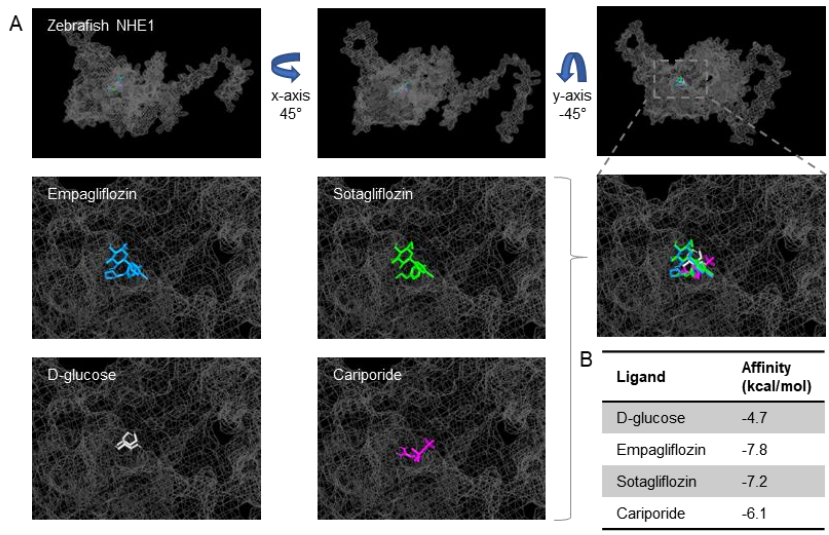


| Ligand | Affinity (kcal/mol) |
|---|---|
| D-glucose | -4.7 |
| Empagliflozin | -7.8 |
| Sotagliflozin | -7.2 |
| Cariporide | -6.1 |

**Figure 15.** Empagliflozin and Sotagliflozin structurally bind to zebrafish NHE1 *in silico.* (A and B) Molecular docking analysis of Empagliflozin, Sotagliflozin, Cariporide and D-glucose binding to a structural model of zebrafish NHE. Empagliflozin is shown in blue, Sotagliflozin is shown in green, Cariporide is in purple, and D-glucose is in gray. D-glucose is served as a negative control, and Cariporide is served as a positive control. (A) Binging site and (B) affinities (kcal/mol).

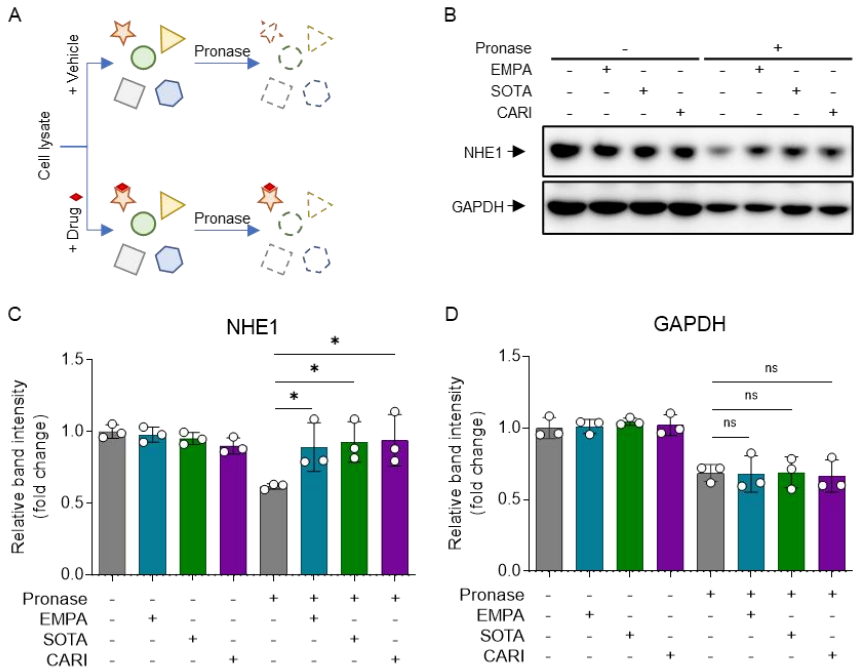


**Figure 16.** Empagliflozin and Sotagliflozin structurally bind to zebrafish NHE1 *in vitro*. (A) Schematic of the drug affinity responsive target stability (DARTS) assay *in vitro*. (B–D) DARTS analysis via immunoblotting using (B and C) NHE1 and (B and D) GAPDH antibody. Data are presented as mean ± standard deviation and each dot represents the value of each experiment. $*p < 0.05$ vs. indicated group.

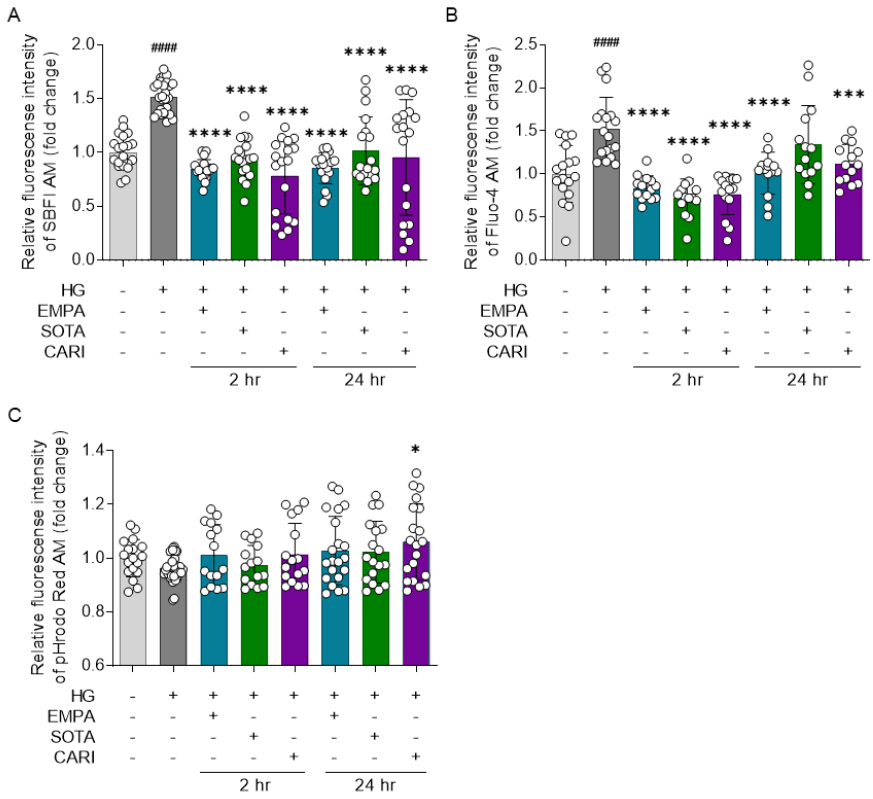


**Figure 17.** Empagliflozin and sotagliflozin functionally inhibit zebrafish NHE1 *in vitro*. (A) Measurement of intracellular $Na^+$, (B) $Ca^{2+}$ and (C) $H^+$ for the analysis of the NHE1 function. (A) SBFI AM for intracellular $Na^+$ measurement, (B) Fluo-4 AM for intracellular $Ca^{2+}$ measurement, and (C) pHrodo Red AM for intracellular $H^+$ measurement (n = 14-35). Data are presented as mean ± standard deviation and each dot represents the value of each sample. $*p < 0.05$, $****p < 0.0001$ vs. HG group, $^{####}p < 0.0001$ vs. control group.

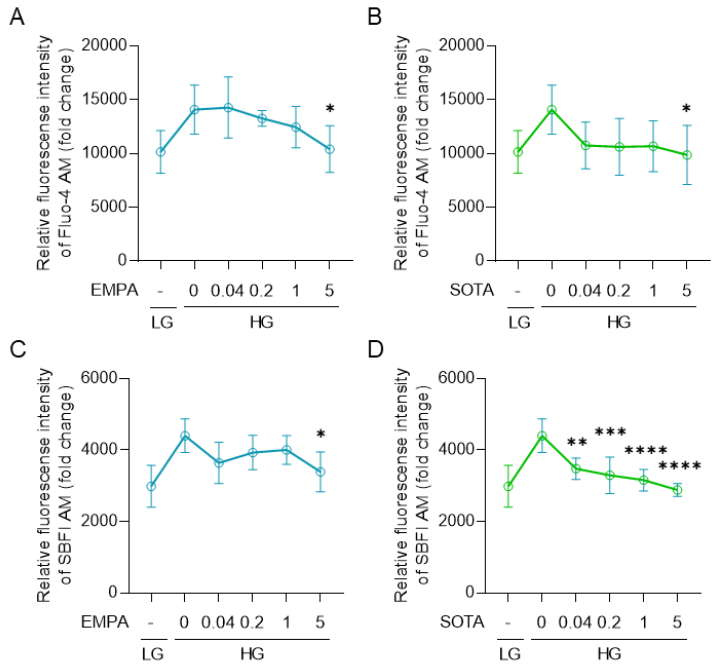


**Figure 18.** Inhibition of intracellular ion changes by Empagliflozin or Sotagliflozin in a concentration-dependent manner. (A) Intracellular $Ca^{2+}$ measurement treated with Empagliflozin or (B) Sotagliflozin. (C) Intracellular $Na^{+}$ measurement treated with Empagliflozin or (D) Sotagliflozin (n = 6-8). Data are presented as mean ± standard deviation and each dot represents the value of each sample. $*p < 0.05$, $**p < 0.01$, $****p < 0.0001$ vs. vehicle group.

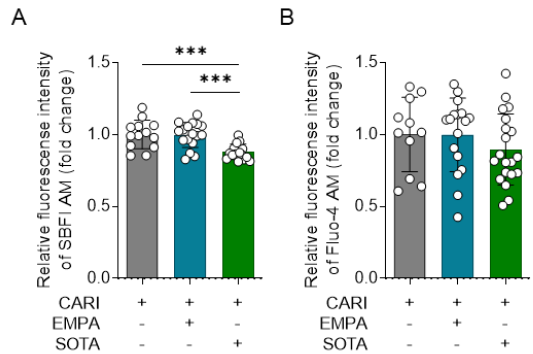


**Figure 19.** Competitive Inhibitory Effects of Cariporide and Empagliflozin or Sotagliflozin. (A) intracellular Na+ and (B) Ca2+ changes in cells treated with Empagliflozin or Sotagliflozin after Cariporide treatment (n = 13−18). Data are presented as mean ± standard deviation and each dot represents the value of each sample. ***$p < 0.001$ vs. vehicle group.

# Discussion

This study presents a method for establishing and evaluating a new zebrafish model for *in vivo* experiments of DM-HFrEF and, through this zebrafish model, provides new insights into the effects of SGLT2 inhibitor, EMPA, and dual SGLT1/2 inhibitor, SOTA, in protecting against DM-HFrEF. First, at the same molarity, EMPA and SOTA provided similar cardioprotective, motility, and survival conservation effects; overall, SOTA was superior to EMPA, although the difference was not significant at lower concentrations. Moreover, the expected significant additive cardioprotective effect of SOTA was not observed in the DM-HFrEF zebrafish model. Second, the morphological abnormality and sharp decrease in survival rate observed at high SOTA concentrations imply the possibility of side effects of SOTA in zebrafish larvae. Third, both EMPA and SOTA inhibited NHE1 structurally and functionally, which may be the main mechanism underlying their cardioprotective effect.

In the previous DM zebrafish larvae models, hyperglycemia was induced by immersion in only GLU[95, 96]. However, according to the results of our study, immersion in high GLU concentrations resulted in a sharp decrease in the survival rates of zebrafish

larvae. This finding indicates that a high-concentration GLU immersion-induced hyperglycemia model is challenging to use in a study requiring a period of 3 days or more and may lead to serious bias in the results. I examined the survival rates of zebrafish at various GLU concentrations and determined an optimum concentration that did not affect viability. Our experimental results show that insulin expression is decreased in GLU/STZ-treated zebrafish larvae without affecting the morphology and maturation of pancreatic $\beta$-cells. It seems that continuous stress caused by GLU and mild damage caused by STZ caused partial dysfunction without destroying $\beta$-cells. In addition, GLU/STZ treatment considerably increased PEPCK and decreased insulin level compared with GLU alone. The increase in PEPCK expression suggests that gluconeogenesis was increased due to the lack of glucose required for tissue metabolism despite the high blood glucose levels. Additionally, the GLU challenge experiment revealed that GLU/STZ treatment reduced glucose homeostasis. These results validated the establishment of a new DM zebrafish model with hyperglycemia and abnormal glucose homeostasis. In this study, DM zebrafish were treated with TER to induce HF. In zebrafish larvae, treatment with TER, a potassium channel blocker, induces HF by reducing cardiac function regardless of cardiac myocardial infarction or injury, thus

showing the characteristics of chronic HF. The present study showed that despite treatment with the same TER concentration, more severe cardiac dysfunction was induced in DM zebrafish than in non-DM zebrafish. In DM zebrafish treated with TER, cardiac contractility significantly decreased, irregular contraction remarkably increased; additionally, a sharp increase in the expression of *nppb*, an HF biomarker, and significant reduction in motility and survival were observed. These results support the results of clinical studies in which patients with DM showed significantly increased HF prevalence and mortality[50, 53].

The newly developed diabetes drugs, an SGLT2 inhibitor and dual SGLT1/2 inhibitor, provide an effective blood-glucose-lowering effect through a unique mechanism[59, 70]. In addition, various beneficial effects such as inhibition of inflammation and senescence have been reported[62-64, 97]. SGLT inhibitors, apart from existing diabetes drugs, are an excellent cardioprotective effect. According to the EMPA-REG and the SOLOIST trial, both drugs dramatically reduced hospitalization of HF and mortality in DM patients[56, 58]. In addition, in the experimental results using a DM animal model, treatment with EMPA and SOTA preserves cardiac function by inhibiting myocardium fibrosis, hypertrophy, and inflammation[98, 99].

However, studies comparing the cardioprotective effects of EMPA and SOTA are still very insufficient. Therefore, I compared the beneficial effects of these two drugs, focusing on the cardioprotective effect. The results of this study using the DM-HF zebrafish model show that the treatment of the two drugs has a remarkable and similar cardioprotective effect and, motility and survival rate improvement effect. Since SGLT2 is not expressed in the heart, several studies on the mechanism of the cardioprotective effect of SGLT2 inhibitors have focused on fluid homeostasis, blood glucose control, or off-target molecules such as NHE1[71-73]. SGLT family unidirectionally transfers glucose and sodium. It plays an important role in regulating fluid homeostasis. However, in this study, edema due to changes in body fluid homeostasis was not observed. Also, changes in insulin and PEPCK related to glucose metabolism were not observed. Therefore, this study focused on NHE1, an off-target molecule of the SGLT2 inhibitor. Several studies suggest that SGLT2 inhibitors directly target NHE1, and NHE1 inhibition by SGLT2 inhibitors suppress NLRP3 inflammasome activation[100] and autophagic cell death in cardiomyocyte[72]. Therefore, the inhibition of NHE1 of SGLT2 inhibitors is one of the crucial mechanisms of cardioprotective effect. I demonstrated that EMPA and SOTA effectively bind and

inhibit to zebrafish NHE1 through *in silico* and *in vitro* experiments. These results are consistent with a recent finding that SGLT2 inhibitors can directly inhibit NHE1[71, 73], providing new evidence that dual SGLT1/2 inhibitors can directly inhibit NHE1. This also suggests that the mechanism of the cardioprotective effect of both EMPA and SOTA is through NHE1 inhibition.

SOTA is the first dual SGLT1/2 inhibitor with at high selectivity for both SGLT1 and 2[70]. SGLT1 is expressed in the myocardium[101]. SGLT1 in cardiomyocytes contributes to glucose uptake and plays an essential role in pathological heart conditions[67]. SGLT1 inhibition helps decrease myocardial hypertrophy and fibrosis[69]. As such, SOTA is expected to provide the cardioprotective effect as same mechanism of SGLT2 inhibitors, in addition to a cardioprotective effect through SGLT1 inhibition, therefore offering a higher cardioprotective effect than the SGLT2 inhibitors. However, in our study, two inhibitors showed similar cardioprotective effect and survival rate improvement at various molarities (0.04–5 $\mu$M). A difference between the two drugs was observed in vFS, one of the cardiac function evaluation parameters. EMPA peaked at 5 $\mu$M, while

SOTA showed a peak value at 1 μM. Treatment with 1 μM SOTA showed a higher vFS than treatment with the same concentration of EMPA, but the difference was not significant. Although SOTA inhibits SGLT1, the similarly confirmed cardioprotective effects of the two drugs suggest that NHE1 inhibition rather than SGLT1 inhibition is the main mechanism behind this effect in the DM-HFrEF zebrafish model. However, further studies are needed to analyze the contribution of NHE1 and SGLT1 inhibition in cardiac function protection. In clinical practice, the doses of both drugs are given as 10 and 25 mg EMPA or 200 mg SOTA based on clinical trials for DM patients[102, 103]. Despite the clinical use of much higher doses of SOTA than EMPA, our study results show that both drugs provide a significant cardioprotective effect even at low molarities. In addition, the high molarity of SOTA significantly decreased the survival rate compared to the same molarity of EMPA, and epicardial edema and uninflated swim bladder were observed. These results suggest that treatment with high molarity of SOTA may have a potential side effect in zebrafish. Since SGLT1 is expressed in the heart, small intestine, and brain and plays a role in absorbing sodium and glucose, it is possible that high concentration SOTA inhibited the minimum glucose absorption required in the heart and intestine. In addition, SGLT2 inhibitors can

reduce cell viability at high concentrations, which can lead to reduced survival rates[62]. Furthermore, although the swim bladder in zebrafish is evolutionarily homologous to the mammalian lung[104], however, it is unclear whether SOTA-induced swim bladder abnormalities in zebrafish are associated with mammalian lung toxicity, so further studies are needed.

The glucose metabolism abnormality is one of the critical risk factors that contribute to the development of HF. Since the heart, which sustained beating, requires large amounts of glucose, glucose homeostasis is essential for cardiac function. Since both EMPA and SOTA effectively control blood glucose, they may alleviate the aggravating effect of HF caused by glucose metabolism abnormality in the DM-HFrEF zebrafish model. Existing studies could not exclude the possibility of a cardioprotective impact due to the improved glucose metabolism, so it was not possible to clarify whether the cardioprotective effect was due to the enhancement of glucose homeostasis. In our results, treatment with EMPA or SOTA improved the survival rate and cardiac function and dramatically decreased the B-type natriuretic peptide levels without affecting the expression of insulin and PEPCK expression in DM-HFrEF zebrafish model. Therefore, it is suggested that the cardioprotective effect

confirmed in the DM-HFrEF zebrafish model is through a mechanism different from glucose metabolism, which makes it possible to consider once again the effect of NHE1 inhibition of EMPA or SOTA mentioned above.

NHE1, which is expected to be an off-target of SGLT2 inhibitors, plays a role in regulating intracellular pH homeostasis by exchanging $Na^+$ and $H^+$. Induction of NHE1 expression and activation are increased by DM-related stimuli such as hyperglycemia and insulin[74, 75]. NHE1 contributes to vascular abnormalities such as retinopathy and atherosclerosis in organ dysfunction and damage caused by diabetes[76, 77]. Upregulation of NHE1 is found not only in DM but also in the ventricular tissue of patients with HF[78]. In addition, selective inhibition of NHE1 improves cardiac function by inhibiting fibrosis and cardiac hypertrophy in an experimental HF model[79, 80]. These reports suggest that NHE1 is a molecule that plays an essential role in the pathogenesis of DM-HF and has potential as a novel target for therapeutic strategies for DM-HF. I showed that both EMPA and SOTA structurally bind to NHE1 and inhibit its functions both *in silico* and *in vitro*. In addition, after NHE1 was inhibited by CARI, the NHE1 inhibitory effect by EMPA or SOTA was not observed. These results not only support several previous studies[71, 73],

but also provide the first evidence that, similar to the SGLT2 inhibitor EMPA, the dual SGLT 1/2 inhibitor SOTA directly inhibits NHE1. The mechanism of the cardioprotective effect of SGLT2 inhibitors is not yet fully understood. In addition to the fact that SGLT2 inhibitor inhibits NHE1, a series of intracellular signaling such as AMPK, mTOR, STAT3 and NLRP3 inflammasome has been reported to some extent[63, 100, 105, 106], but it is not clear how NHE1 inhibition induces these intracellular changes. Activation of NHE1 increases intracellular $Na^+$ by exchanging intracellular $H^+$. The increased intracellular $Na^+$ is again exchanged with $Ca^{2+}$ through NCX, resulting in the accumulation of intracellular $Ca^{2+}$[79]. Intracellular $Ca^{2+}$ accumulation is potentially cytotoxic and can cause apoptosis[107, 108]. SGLT2 inhibitors may be able to regulate intracellular $Ca^{2+}$ through NHE1 inhibition. In fact, according to previous reports, treatment with SGLT2 inhibitors in cardiomyocytes inhibited the accumulation of intracellular $Ca^{2+}$[109], which is also confirmed by our results. In addition, SGLT2 inhibitor may regulate intracellular $Ca^{2+}$ by directly inhibiting NCX[106]. These suggest that SGLT2 inhibitors inhibit NHE1 and that intracellular $Ca^{2+}$ regulation may be a key mechanism of beneficial effects.

This study has various limitations. First, although the zebrafish

used as a model animal in this study has various advantages, it may be difficult to apply to humans because it is a non-mammal. Insights gained from larval zebrafish studies require testing mammalian model animals to determine evolutionary conservation and interspecies differences. Second, DM-HFrEF zebrafish models pertain to HF with reduced ejection fraction and do not apply to HF with preserved ejection fraction, which constitutes approximately 40% of the overall HF cases. Third, since this model uses larvae that have not completely developed, the structure of the heart is very simple, so myocardial fibrosis and hypertrophy, which are typical features of DM-HF, are not observed. In addition, in TER-induced HF, inflammatory responses and changes in immune cells are not observed. Fourth, the exact mechanism of the cardioprotective effect of SGLT inhibitors has not been elucidated. Although the focus was on the inhibition of NHE1, in order to elucidate the exact molecular mechanism of the cardioprotective effect, it is necessary to study more precise interactions through loss-of-function or gain-of-function experiments on NHE1, NCX, SGLT1, and SGLT2. Fourth, inhibition of SGLT inhibitors on NHE1 was confirmed only in cardiomyocytes, but it is necessary to confirm the effects of SGLT inhibitors in various cells such as endothelial cells and immune cells constituting the heart. Finally, the

cause of the decreased survival and morphological abnormalities observed in the high-dose SOTA-treated group has not been elucidated. Understanding the cause will contribute to the development of more effective drugs and less side-effects, so further research is needed.

In conclusion, this study established a novel animal model for DM-HF by sequentially immersing zebrafish larvae in GLU/STZ and TER, and presented a method to evaluate DM-HF. In addition, study using a zebrafish model of DM-HFrEF show that SGLT2 inhibitors and dual SGLT1/2 inhibitors provide similar cardioprotective effects. No significant differences in protective effects were observed due to the expected SGLT1 inhibition by dual SGLT1/2 inhibitors. However, both inhibitors showed a high affinity for NHE1. Therefore, I propose that NHE1 inhibition is an essential mechanism for the cardioprotective effects of SGLT2 and dual SGLT1/2 inhibitors. This study will help researchers understand the mechanisms by which SGLT2 inhibitors and dual SGLT1/2 inhibitors affect DM-HFrEF and provide important information about the potential benefits of these inhibitors for DM patients with HF.

# Bibliography


1. *Cardiovascular diseases*. Available from: https://www.who.int/health-topics/cardiovascular-diseases.
2. Mensah, G.A. and D.W. Brown, *An overview of cardiovascular disease burden in the United States.* Health Aff (Millwood), 2007. **26**(1): p. 38-48.
3. Go, A.S., et al., *Heart disease and stroke statistics--2014 update: a report from the American Heart Association.* Circulation, 2014. **129**(3): p. e28-e292.
4. Yazdanyar, A. and A.B. Newman, *The burden of cardiovascular disease in the elderly: morbidity, mortality, and costs.* Clin Geriatr Med, 2009. **25**(4): p. 563-77, vii.
5. Ravingerová, T., et al., *Pleiotropic preconditioning-like cardioprotective effects of hypolipidemic drugs in acute ischemia-reperfusion in normal and hypertensive rats.* Canadian Journal of Physiology and Pharmacology, 2015. **93**(7): p. 495-503.
6. Stearns, F.W., *One hundred years of pleiotropy: a retrospective.* Genetics, 2010. **186**(3): p. 767-73.
7. Rizos, C.V., M.S. Elisaf, and E.N. Liberopoulos, *Are the pleiotropic effects of telmisartan clinically relevant?* Curr Pharm Des, 2009. **15**(24): p. 2815-32.
8. Wang, R., et al., *Pleiotropic effects of the beta-adrenoceptor blocker carvedilol on calcium regulation during oxidative stress-induced apoptosis in cardiomyocytes.* J Pharmacol Exp Ther, 2006. **318**(1): p. 45-52.
9. Bauriedel, G., et al., *Antiplatelet effects of angiotensin-converting enzyme inhibitors compared with aspirin and clopidogrel: a pilot study with whole-blood aggregometry.* Am Heart J, 2003. **145**(2): p. 343-8.
10. Oesterle, A., U. Laufs, and J.K. Liao, *Pleiotropic Effects of Statins*

*on the Cardiovascular System.* Circ Res, 2017. **120**(1): p. 229-243.

11. Kang, S.M. and J.H. Park, *Pleiotropic Benefits of DPP-4 Inhibitors Beyond Glycemic Control.* Clin Med Insights Endocrinol Diabetes, 2021. **14**: p. 11795514211051698.
12. Liu, W., et al., *Pleiotropic Effects of Metformin on the Antitumor Efficiency of Immune Checkpoint Inhibitors.* Front Immunol, 2020. **11**: p. 586760.
13. Goldberg, L.R., *The Pleiotropic Effects of SGLT2 Inhibitors: Remodeling the Treatment of Heart Failure.* J Am Coll Cardiol, 2021. **77**(3): p. 256-258.
14. Kim, I., C.S. Park, and H.Y. Lee, *Angiotensin II Type 1 Receptor Blocker, Fimasartan, Reduces Vascular Smooth Muscle Cell Senescence by Inhibiting the CYR61 Signaling Pathway.* Korean Circ J, 2019. **49**(7): p. 615-626.
15. Costantino, S., F. Paneni, and F. Cosentino, *Ageing, metabolism and cardiovascular disease.* J Physiol, 2016. **594**(8): p. 2061-73.
16. Minamino, T., et al., *Endothelial cell senescence in human atherosclerosis: role of telomere in endothelial dysfunction.* Circulation, 2002. **105**(13): p. 1541-4.
17. Campisi, J. and F. d'Adda di Fagagna, *Cellular senescence: when bad things happen to good cells.* Nat Rev Mol Cell Biol, 2007. **8**(9): p. 729-40.
18. Nilsson, P.M., et al., *Early vascular ageing in translation: from laboratory investigations to clinical applications in cardiovascular prevention.* J Hypertens, 2013. **31**(8): p. 1517-26.
19. Harley, C.B., A.B. Futcher, and C.W. Greider, *Telomeres shorten during ageing of human fibroblasts.* Nature, 1990. **345**(6274): p. 458-60.
20. Dimri, G.P., et al., *A biomarker that identifies senescent human cells in culture and in aging skin in vivo.* Proc Natl Acad Sci U S A, 1995. **92**(20): p. 9363-7.
21. Serrano, M., et al., *Oncogenic ras provokes premature cell*

*senescence associated with accumulation of p53 and p16INK4a.* Cell, 1997. **88**(5): p. 593-602.

22. Zhou, M.S., et al., *Reduced NAD(P)H oxidase in low renin hypertension: link among angiotensin II, atherogenesis, and blood pressure.* Hypertension, 2006. **47**(1): p. 81-6.
23. Anderson, S., F.F. Jung, and J.R. Ingelfinger, *Renal renin-angiotensin system in diabetes: functional, immunohistochemical, and molecular biological correlations.* Am J Physiol, 1993. **265**(4 Pt 2): p. F477-86.
24. Weber, K.T. and C.G. Brilla, *Pathological hypertrophy and cardiac interstitium. Fibrosis and renin-angiotensin-aldosterone system.* Circulation, 1991. **83**(6): p. 1849-65.
25. Kranzhofer, R., et al., *Angiotensin induces inflammatory activation of human vascular smooth muscle cells.* Arterioscler Thromb Vasc Biol, 1999. **19**(7): p. 1623-9.
26. Shim, K.Y., et al., *Role of the renin-angiotensin system in hepatic fibrosis and portal hypertension.* Korean J Intern Med, 2018. **33**(3): p. 453-461.
27. Kunieda, T., et al., *Angiotensin II induces premature senescence of vascular smooth muscle cells and accelerates the development of atherosclerosis via a p21-dependent pathway.* Circulation, 2006. **114**(9): p. 953-60.
28. de Cavanagh, E.M., F. Inserra, and L. Ferder, *Angiotensin II blockade: a strategy to slow ageing by protecting mitochondria?* Cardiovasc Res, 2011. **89**(1): p. 31-40.
29. Basso, N., et al., *Protective effect of long-term angiotensin II inhibition.* Am J Physiol Heart Circ Physiol, 2007. **293**(3): p. H1351-8.
30. Li, Y.W., et al., *AT1 Receptor Modulator Attenuates the Hypercholesterolemia-Induced Impairment of the Myocardial Ischemic Post-Conditioning Benefits.* Korean Circ J, 2017. **47**(2): p. 182-192.

31. Jo, Y.I., et al., *Effect of low-dose valsartan on proteinuria in normotensive immunoglobulin A nephropathy with minimal proteinuria: a randomized trial.* Korean J Intern Med, 2016. **31**(2): p. 335-43.
32. Lee, J.H., et al., *Angiotensin II type 1 receptor blockers as a first choice in patients with acute myocardial infarction.* Korean J Intern Med, 2016. **31**(2): p. 267-76.
33. Garg, N., P. Krishan, and A. Syngle, *Angiotensin-Receptor Blockade Improves Inflammation and Endothelial Dysfunction in Ankylosing Spondylitis: ARB-AS Study.* Int J Angiol, 2021. **30**(4): p. 262-270.
34. Kim, T.W., et al., *Synthesis and antihypertensive activity of pyrimidin-4(3H)-one derivatives as losartan analogue for new angiotensin II receptor type 1 (AT1) antagonists.* Bioorg Med Chem Lett, 2012. **22**(4): p. 1649-54.
35. Sim, D.S., et al., *Cardioprotective effect of fimasartan, a new angiotensin receptor blocker, in a porcine model of acute myocardial infarction.* J Korean Med Sci, 2015. **30**(1): p. 34-43.
36. Yang, X.L., et al., *Anti-inflammatory effects of fimasartan via Akt, ERK, and NFkappaB pathways on astrocytes stimulated by hemolysate.* Inflamm Res, 2016. **65**(2): p. 115-23.
37. Quan, H., et al., *Fimasartan, an angiotensin II receptor antagonist, ameliorates an in vivo zebrafish model of heart failure.* Korean J Intern Med, 2020. **35**(6): p. 1400-1410.
38. Hilfiker, A., et al., *Expression of CYR61, an angiogenic immediate early gene, in arteriosclerosis and its regulation by angiotensin II.* Circulation, 2002. **106**(2): p. 254-60.
39. Lau, L.F. and S.C. Lam, *The CCN family of angiogenic regulators: the integrin connection.* Exp Cell Res, 1999. **248**(1): p. 44-57.
40. O'Brien, T.P., et al., *Expression of cyr61, a growth factor-inducible immediate-early gene.* Mol Cell Biol, 1990. **10**(7): p. 3569-77.
41. Babic, A.M., et al., *CYR61, a product of a growth factor-inducible*

*immediate early gene, promotes angiogenesis and tumor growth.* Proc Natl Acad Sci U S A, 1998. **95**(11): p. 6355-60.

42. Lee, H.Y., et al., *Forkhead transcription factor FOXO3a is a negative regulator of angiogenic immediate early gene CYR61, leading to inhibition of vascular smooth muscle cell proliferation and neointimal hyperplasia.* Circ Res, 2007. **100**(3): p. 372-80.
43. Jun, J.I. and L.F. Lau, *The matricellular protein CCN1 induces fibroblast senescence and restricts fibrosis in cutaneous wound healing.* Nat Cell Biol, 2010. **12**(7): p. 676-85.
44. Feng, T., et al., *CCN1-Induced Cellular Senescence Promotes Heart Regeneration.* Circulation, 2019. **139**(21): p. 2495-2498.
45. Du, J., et al., *Aging increases CCN1 expression leading to muscle senescence.* Am J Physiol Cell Physiol, 2014. **306**(1): p. C28-36.
46. Lee, S.J. and S.H. Park, *Arterial ageing.* Korean Circ J, 2013. **43**(2): p. 73-9.
47. Min, L.J., et al., *Signaling mechanisms of angiotensin II in regulating vascular senescence.* Ageing Res Rev, 2009. **8**(2): p. 113-21.
48. Tsai, I.C., et al., *Reactive oxygen species derived from NADPH oxidase 1 and mitochondria mediate angiotensin II-induced smooth muscle cell senescence.* J Mol Cell Cardiol, 2016. **98**: p. 18-27.
49. Federation, I.D., *IDF Diabetes Atlas 10th edition*. 2021.
50. McMurray, J.J.V., et al., *Heart failure: a cardiovascular outcome in diabetes that can no longer be ignored.* The Lancet Diabetes & Endocrinology, 2014. **2**(10): p. 843-851.
51. Holman, R.R., et al., *10-year follow-up of intensive glucose control in type 2 diabetes.* N Engl J Med, 2008. **359**(15): p. 1577-89.
52. Rorth, R., et al., *Risk of Incident Heart Failure in Patients With Diabetes and Asymptomatic Left Ventricular Systolic Dysfunction.* Diabetes Care, 2018. **41**(6): p. 1285-1291.
53. Kong, M.G., et al., *Impact of diabetes mellitus on mortality in patients with acute heart failure: a prospective cohort study.*

Cardiovasc Diabetol, 2020. **19**(1): p. 49.

54. Jang, S.Y., et al., *Impact of insulin therapy on the mortality of acute heart failure patients with diabetes mellitus.* Cardiovasc Diabetol, 2021. **20**(1): p. 180.

55. *Guidance for Industry Diabetes Mellitus — Evaluating Cardiovascular Risk in New Antidiabetic Therapies to Treat Type 2 Diabetes*, in *U.S. Department of Health and Human Services Food and Drug Administration Center for Drug Evaluation and Research (CDER)*. 2008. p. 8.

56. Zinman, B., et al., *Empagliflozin, Cardiovascular Outcomes, and Mortality in Type 2 Diabetes.* N Engl J Med, 2015. **373**(22): p. 2117-28.

57. Wiviott, S.D., et al., *The design and rationale for the Dapagliflozin Effect on Cardiovascular Events (DECLARE)-TIMI 58 Trial.* Am Heart J, 2018. **200**: p. 83-89.

58. Bhatt, D.L., et al., *Sotagliflozin in Patients with Diabetes and Recent Worsening Heart Failure.* N Engl J Med, 2021. **384**(2): p. 117-128.

59. Chao, E.C. and R.R. Henry, *SGLT2 inhibition--a novel strategy for diabetes treatment.* Nat Rev Drug Discov, 2010. **9**(7): p. 551-9.

60. Uhlen, M., et al., *Proteomics. Tissue-based map of the human proteome.* Science, 2015. **347**(6220): p. 1260419.

61. McMurray, J.J.V., K.F. Docherty, and P.S. Jhund, *Dapagliflozin in Patients with Heart Failure and Reduced Ejection Fraction. Reply.* N Engl J Med, 2020. **382**(10): p. 973.

62. Abdollahi, E., et al., *Dapagliflozin exerts anti-inflammatory effects via inhibition of LPS-induced TLR-4 overexpression and NF-κB activation in human endothelial cells and differentiated macrophages.* Eur J Pharmacol, 2022. **918**: p. 174715.

63. Lee, T.M., N.C. Chang, and S.Z. Lin, *Dapagliflozin, a selective SGLT2 Inhibitor, attenuated cardiac fibrosis by regulating the macrophage polarization via STAT3 signaling in infarcted rat hearts.* Free Radic Biol Med, 2017. **104**: p. 298-310.

64. Madonna, R., et al., *Empagliflozin reduces the senescence of cardiac stromal cells and improves cardiac function in a murine model of diabetes.* J Cell Mol Med, 2020. **24**(21): p. 12331-12340.
65. Braunwald, E., *Gliflozins in the Management of Cardiovascular Disease.* N Engl J Med, 2022. **386**(21): p. 2024-2034.
66. Turk, E., et al., *Glucose/galactose malabsorption caused by a defect in the Na+/glucose cotransporter.* Nature, 1991. **350**(6316): p. 354-6.
67. Banerjee, S.K., et al., *SGLT1 is a novel cardiac glucose transporter that is perturbed in disease states.* Cardiovasc Res, 2009. **84**(1): p. 111-8.
68. Ferte, L., et al., *New insight in understanding the contribution of SGLT1 in cardiac glucose uptake: evidence for a truncated form in mice and humans.* Am J Physiol Heart Circ Physiol, 2021. **320**(2): p. H838-H853.
69. Matsushita, N., et al., *Chronic Pressure Overload Induces Cardiac Hypertrophy and Fibrosis via Increases in SGLT1 and IL-18 Gene Expression in Mice.* Int Heart J, 2018. **59**(5): p. 1123-1133.
70. Zambrowicz, B., et al., *LX4211, a dual SGLT1/SGLT2 inhibitor, improved glycemic control in patients with type 2 diabetes in a randomized, placebo-controlled trial.* Clin Pharmacol Ther, 2012. **92**(2): p. 158-69.
71. Uthman, L., et al., *Class effects of SGLT2 inhibitors in mouse cardiomyocytes and hearts: inhibition of Na(+)/H(+) exchanger, lowering of cytosolic Na(+) and vasodilation.* Diabetologia, 2018. **61**(3): p. 722-726.
72. Jiang, K., et al., *Cardioprotective mechanism of SGLT2 inhibitor against myocardial infarction is through reduction of autosis.* Protein Cell, 2022. **13**(5): p. 336-359.
73. Zuurbier, C.J., et al., *Sodium-glucose co-transporter 2 inhibitor empagliflozin inhibits the cardiac Na+/H+ exchanger 1: persistent inhibition under various experimental conditions.* Cardiovasc Res,

2021. **117**(14): p. 2699-2701.

74. Jandeleit-Dahm, K., et al., *Diabetes-induced vascular hypertrophy is accompanied by activation of Na(+)-H(+) exchange and prevented by Na(+)-H(+) exchange inhibition.* Circ Res, 2000. **87**(12): p. 1133-40.

75. Ganz, M.B., K. Hawkins, and R.F. Reilly, *High glucose induces the activity and expression of Na(+)/H(+) exchange in glomerular mesangial cells.* Am J Physiol Renal Physiol, 2000. **278**(1): p. F91-6.

76. Cukiernik, M., et al., *The role of the sodium hydrogen exchanger-1 in mediating diabetes-induced changes in the retina.* Diabetes Metab Res Rev, 2004. **20**(1): p. 61-71.

77. Madonna, R. and R. De Caterina, *Aquaporin-1 and sodium-hydrogen exchangers as pharmacological targets in diabetic atherosclerosis.* Curr Drug Targets, 2015. **16**(4): p. 361-5.

78. Trum, M., et al., *Empagliflozin inhibits Na(+) /H(+) exchanger activity in human atrial cardiomyocytes.* ESC Heart Fail, 2020. **7**(6): p. 4429-37.

79. Nakamura, T.Y., et al., *Activation of Na+/H+ exchanger 1 is sufficient to generate Ca2+ signals that induce cardiac hypertrophy and heart failure.* Circ Res, 2008. **103**(8): p. 891-9.

80. Kilić, A., et al., *Early and transient sodium-hydrogen exchanger isoform 1 inhibition attenuates subsequent cardiac hypertrophy and heart failure following coronary artery ligation.* J Pharmacol Exp Ther, 2014. **351**(3): p. 492-9.

81. Parng, C., et al., *Zebrafish: a preclinical model for drug screening.* Assay Drug Dev Technol, 2002. **1**(1 Pt 1): p. 41-8.

82. Grunwald, D.J. and G. Streisinger, *Induction of recessive lethal and specific locus mutations in the zebrafish with ethyl nitrosourea.* Genet Res, 1992. **59**(2): p. 103-16.

83. Jurczyk, A., et al., *Dynamic glucoregulation and mammalian-like responses to metabolic and developmental disruption in zebrafish.*

Gen Comp Endocrinol, 2011. **170**(2): p. 334-45.

84. Howe, K., et al., *The zebrafish reference genome sequence and its relationship to the human genome.* Nature, 2013. **496**(7446): p. 498-503.

85. Missinato, M.A., et al., *Zebrafish heart regenerates after chemoptogenetic cardiomyocyte depletion.* Dev Dyn, 2021. **250**(7): p. 986-1000.

86. Huang, C.J., et al., *Germ-line transmission of a myocardium-specific GFP transgene reveals critical regulatory elements in the cardiac myosin light chain 2 promoter of zebrafish.* Dev Dyn, 2003. **228**(1): p. 30-40.

87. Kim, I., S.H. Seok, and H.Y. Lee, *Development of a Zebrafish Larvae Model for Diabetic Heart Failure With Reduced Ejection Fraction.* Korean Circ J, 2023. **53**(1): p. 34-46.

88. Underwood, W. and R. Anthony, *AVMA guidelines for the euthanasia of animals: 2020 edition.* Retrieved on March, 2020. **2013**(30): p. 2020-1.

89. diIorio, P.J., et al., *Sonic hedgehog is required early in pancreatic islet development.* Dev Biol, 2002. **244**(1): p. 75-84.

90. Steven, W., et al. *AVMA guidelines for the euthanasia of animals: 2020 edition*. 2020. American Veterinary Medical Association Schaumburg, IL.

91. Varadi, M., et al., *AlphaFold Protein Structure Database: massively expanding the structural coverage of protein-sequence space with high-accuracy models.* Nucleic Acids Res, 2022. **50**(D1): p. D439-D444.

92. Trott, O. and A.J. Olson, *AutoDock Vina: improving the speed and accuracy of docking with a new scoring function, efficient optimization, and multithreading.* J Comput Chem, 2010. **31**(2): p. 455-61.

93. Lomenick, B., et al., *Target identification using drug affinity responsive target stability (DARTS).* Proc Natl Acad Sci U S A,

2009. **106**(51): p. 21984-9.

94. Bresciani, E., E. Broadbridge, and P.P. Liu, *An efficient dissociation protocol for generation of single cell suspension from zebrafish embryos and larvae.* MethodsX, 2018. **5**: p. 1287-1290.

95. Lee, Y. and J. Yang, *Development of a zebrafish screening model for diabetic retinopathy induced by hyperglycemia: Reproducibility verification in animal model.* Biomed Pharmacother, 2021. **135**: p. 111201.

96. Singh, A., et al., *High glucose levels affect retinal patterning during zebrafish embryogenesis.* Sci Rep, 2019. **9**(1): p. 4121.

97. Kim, M.N., J.H. Moon, and Y.M. Cho, *Sodium-glucose cotransporter-2 inhibition reduces cellular senescence in the diabetic kidney by promoting ketone body-induced NRF2 activation.* Diabetes Obes Metab, 2021. **23**(11): p. 2561-2571.

98. Grempler, R., et al., *Empagliflozin, a novel selective sodium glucose cotransporter-2 (SGLT-2) inhibitor: characterisation and comparison with other SGLT-2 inhibitors.* Diabetes Obes Metab, 2012. **14**(1): p. 83-90.

99. Young, S.L., et al., *Sotagliflozin, a Dual SGLT1/2 Inhibitor, Improves Cardiac Outcomes in a Normoglycemic Mouse Model of Cardiac Pressure Overload.* Front Physiol, 2021. **12**: p. 738594.

100. Kim, S.R., et al., *SGLT2 inhibition modulates NLRP3 inflammasome activity via ketones and insulin in diabetes with cardiovascular disease.* Nat Commun, 2020. **11**(1): p. 2127.

101. Zhou, L., et al., *Human cardiomyocytes express high level of Na+/glucose cotransporter 1 (SGLT1).* J Cell Biochem, 2003. **90**(2): p. 339-46.

102. Kadowaki, T., et al., *Empagliflozin monotherapy in Japanese patients with type 2 diabetes mellitus: a randomized, 12-week, double-blind, placebo-controlled, phase II trial.* Adv Ther, 2014. **31**(6): p. 621-38.

103. Lapuerta, P., et al., *Study design and rationale of a dose-ranging*

*trial of LX4211, a dual inhibitor of SGLT1 and SGLT2, in type 2 diabetes inadequately controlled on metformin monotherapy.* Clin Cardiol, 2013. **36**(7): p. 367-71.

104. Zheng, W., et al., *Comparative transcriptome analyses indicate molecular homology of zebrafish swimbladder and mammalian lung.* PLoS One, 2011. **6**(8): p. e24019.

105. Sun, X., et al., *Empagliflozin Ameliorates Obesity-Related Cardiac Dysfunction by Regulating Sestrin2-Mediated AMPK-mTOR Signaling and Redox Homeostasis in High-Fat Diet-Induced Obese Mice.* Diabetes, 2020. **69**(6): p. 1292-1305.

106. Yu, Y.W., et al., *Sodium-Glucose Co-transporter-2 Inhibitor of Dapagliflozin Attenuates Myocardial Ischemia/Reperfusion Injury by Limiting NLRP3 Inflammasome Activation and Modulating Autophagy.* Front Cardiovasc Med, 2021. **8**: p. 768214.

107. Orrenius, S., B. Zhivotovsky, and P. Nicotera, *Regulation of cell death: the calcium-apoptosis link.* Nat Rev Mol Cell Biol, 2003. **4**(7): p. 552-65.

108. Lynch, K., et al., *Basic fibroblast growth factor inhibits apoptosis of spontaneously immortalized granulosa cells by regulating intracellular free calcium levels through a protein kinase Cdelta-dependent pathway.* Endocrinology, 2000. **141**(11): p. 4209-17.

109. Quagliariello, V., et al., *The SGLT-2 inhibitor empagliflozin improves myocardial strain, reduces cardiac fibrosis and pro-inflammatory cytokines in non-diabetic mice treated with doxorubicin.* Cardiovasc Diabetol, 2021. **20**(1): p. 150.

# Abstract in Korean

약물의 다면발현 효과의 기초가 되는 분자 메커니즘을 이해하는 것은 약물 사용을 최적화하는 데 중요하며, 새로운 치료법의 개발 뿐만 아니라 질병 발병에 대한 이해에 더 기여할 수 있다. 이 연구는 혈관 노화와 당뇨 심부전에 대한 Angiotensin II(Ang II) type 1 receptor blocker (ARB)와 Sodium-Glucose cotransporter (SGLT) inhibitor의 다면발현 효과를 설명한다.

제1장에서는 새로운 ARB인 Fimasartan (FIMA)이 Ang II 유도 세포 노화 메커니즘에 미치는 항노화 효과를 설명한다. Ang II는 혈관 노화를 가속화하는 것으로 제안되었지만 명확한 분자 메커니즘은 알려지지 않았다. Ang II 처리된 인간 관상동맥 평활근 세포(hCASMC)는 senescence-associated $\beta$-galactosidase (SA-$\beta$-gal) 양성 세포가 유의하게 증가했다. 그러나 Ang II에 의해 유도된 세포 노화는 FIMA를 사용한 전처리에 의해 현저하게 감소되었다. 노화의 조절인자인 p53과 p16의 발현은 Ang II에 의해 유의하게 증가되었고 FIMA에 의해 억제되었다. Cellular communication factor 1 (CCN1)의 발현은 Ang II에 의해 빠르게 유도되었다. 대조군과 비교하여, Ad-CCN1 viral vector transfection에 의해 CCN1이 과발현된 hCASMC는 SA-$\beta$-gal 양성 세포가 증가했다. Ad-AS-CCN1 transfection에 의한 CCN1 억제 시 Ang II 유도 노화가 유의하게 감소하였다. Ang II에 의한 p53 발현은 Ad-AS-CCN1에 의해 유의하게 감쇠 된 반면, p16 발현은 조절되지

않았다. Ang II는 FIMA에 의해 유의미하게 차단된 ERK1/2와 p38 MAPK를 활성화하였다. ERK와 p38 억제는 모두 Ang II 유도 CCN1 발현을 조절하였다. 그러나 p53 발현은 ERK1/2에 의해서만 조절되었고, p16 발현은 p38 MAPK에 의해서만 감쇠 되었다. 결론적으로, Ang II는 ERK/p38 MAPK-CCN1-p53 경로에 의해 hCASMCs의 노화를 유도했고, FIMA는 Ang II 유도 세포 노화로부터 보호되었다.

제2장에서는 당뇨병 (Diabetes mellitus, DM) 관련 심부전 (Heart failure, HF)에서 SGLT2 inhibitor인 Empagliflozin (EMPA)과 dual SGLT1/2 inhibitor인 Sotagliflozin (SOTA)의 심장 보호효과 및 분자 메커니즘을 연구하였다. DM-HF는 높은 이환율과 사망률을 유발한다. SGLT inhibitor는 포도당을 낮추는 효능을 넘어 HF 억제 약물로 부상하고 있다. 그러나 이러한 심장 보호 효과의 기초가 되는 정확한 메커니즘은 아직 설명되지 않았다. 여기서, 나는 DM과 ejection fraction이 감소된 HF이 결합된 새로운 제브라피쉬 치어 모델 (DM-HFrEF)에서 EMPA와 SOTA의 효과를 비교하기 위해서 심근 수축 기능, 운동성 및 생존율을 평가했다. DM-HFrEF 제브라피쉬 치어는 심장 수축성 저하와 운동성 및 생존율 저하를 보였으며, 모두 EMPA 또는 SOTA 치료를 통해 개선되었다. 그러나 높은 농도의 SOTA 처치군은 같은 농도의 EMP 처치군에 비해 생존율이 낮고 운동성 보존력이 떨어졌으며, 미팽창된 부레가 관찰되었다. 두 약물이 Sodium-Hydrogen Exchanger 1(NHE1)에 미치는 구조적 결합 및 조절 효과는 *in silico*와 *in vitro*에서 평가되었다. SOTA, EMPA 및 NHE1 inhibitor인 Cariporide (CARI)는 *in*

*silico* 및 *in vitro*에서 NHE1과 유사한 구조적 결합 친화력을 보였다. 또한, EMPA, SOTA, CARI는 NHE1 활성의 억제를 통해 세포내 $H^+$, $Na^+$, $Ca^{2+}$의 변화를 효과적으로 감소시켰으며, CARI로 전처리한 세포에서는 EMPA 또는 SOTA의 NHE1 억제 효과가 관찰되지 않았다. 이러한 결과는 EMPA와 SOTA 모두 NHE1 활성 억제를 통해 DM-HFrEF 제브라피쉬 모델에서 심장 보호효과를 발휘함을 시사한다. 또한 두 약물의 유사한 심장 보호 효과에도 불구하고, SOTA는 고농도에서 EMPA보다 덜 효과적일 수 있다.

**주요어: 다면발현 효과, 노화, 당뇨, 심부전**

**학 번: 2017-24875**